Journal of Petroleum Science and Engineering 211 (2022) 109976

Contents lists available at ScienceDirect

Journal of Petroleum Science and Engineering

journal homepage: www.elsevier.com/locate/petrol

Three-dimensional transient flow in heterogeneous reservoirs: Integral transform solution of a generalized point-source problem

Leonardo O. Pelisoli [a,*], Renato M. Cotta [b,c], Carolina P. Naveira-Cotta [c], Paulo Couto [d]

[a] Petrobras S.A., Rio de Janeiro, Brazil
[b] General Directorate of Nuclear and Technological Development, DGDNTM, Brazilian Navy, Ministry of Defense, RJ, Brazil
[c] Mechanical Eng. Dept., POLI & COPPE, Universidade Federal do Rio de Janeiro, UFRJ, Brazil
[d] Civil Eng. Dept., POLI & COPPE, Universidade Federal do Rio de Janeiro, UFRJ, Brazil

ARTICLE INFO

Keywords:
Integral transforms
Point-source problem
Heterogeneous reservoirs
Pressure transient analysis

ABSTRACT

Appraisal well testing plays a key role in optimizing a complex field's exploitation strategy — and increasing complexity often calls for more elaborate reservoir models for the proper interpretation of each test's results. The classical analytical methods usually require restrictive simplifying assumptions, which limit their usefulness when dealing with reservoir heterogeneity. We seek to solve this issue by applying the hybrid analytical–numerical Generalized Integral Transform Technique (GITT) to the pressure diffusivity equation — and specifically, to the point-source problem extended to a reservoir with arbitrary permeability variation irregularly distributed throughout the 3D domain. The technique is first demonstrated to produce an exact alternative form of the well-known solution to the classical point-source in a homogeneous reservoir. This equivalence is then used to derive a computationally efficient working expression for the generalized point-source in a heterogeneous reservoir. Finally, this building block is applied to construct a uniform flow solution for a limited entry vertical well through spatial superposition — thus demonstrating the usage of the GITT for other wellbore geometries. Synthetic examples are used to show that the obtained expressions are in good agreement with results from a commercial reservoir simulator. In all cases presented, the eigenfunction expansions for both the drawdown pressure and its logarithmic derivative converge to at least four and two significant digits, respectively, within the adopted practical ranges of the series' truncation orders. It is clear that the pressure expansions have better convergence characteristics, which are also influenced by the time value and by the distance from the position under consideration to the point-source. The resulting novel solution to the point-source provided in the present work is the most general and least restrictive expression presented so far to this single problem in a heterogeneous domain, and it is suitable for pressure transient analysis.

1. Introduction

There is no denying that renewable energy's share in the global fuel mix has been rapidly increasing in recent years, as public opinion and environmental policy changes encourage organizations and countries to strive towards reducing CO_2 emissions (Herbert, 2016; IEA, 2021). Nevertheless, oil is still the world's single largest energy source, accounting for one-third of global primary energy consumption (Wachtmeister et al., 2018). Furthermore, the global demand for crude oil has been on an increasing trajectory for the past decade — and despite the momentary setback due to the impacts of the coronavirus pandemic, current projections still point towards continued growth in the coming years (Sönichsen, 2021). Exploration and production costs rise as companies move further offshore or into increased political risk regions (Mabrouk, 2014) and drill towards deeper, more challenging formations — all of which amplify the importance of optimized exploitation strategies. Well testing plays a key role in this regard (Kodhelaj and Shkëqim, 2016): early on, for the acquisition of dynamic data to support the primary and secondary recovery phases; and then later on, for an optimal selection of techniques and candidate wells for enhanced oil recovery (EOR) (Green and Willhite, 1998) — the efficiency of which will be significantly affected by prior knowledge about the heterogeneity of the formation (Zhong et al., 2020). And as the fields' complexity increases, so does the need for increasingly elaborate reservoir models for the proper interpretation of appraisal and reservoir monitoring well testing results.

* Corresponding author.
E-mail address: lopelisoli@petrobras.com.br (L.O. Pelisoli).

https://doi.org/10.1016/j.petrol.2021.109976
Received 25 June 2021; Received in revised form 27 November 2021; Accepted 30 November 2021
Available online 25 December 2021

Table 1
Characteristics and capabilities of several existing models for transient flow in heterogeneous reservoirs, for direct comparison with the present work.

References	Domain	Wellbore geometry	Dimensionality	Heterogeneity
Larsen (1985)	Bounded	Vertical	2D (x, y)	Homogeneous medium with polygon-shaped bounds.
Barenblatt et al. (1960), Warren and Root (1963)	Semi-infinite, Bounded	Vertical	2D (r, θ)	Dual porosity.
Ehlig-Economides and Ayoub (1986)	Semi-infinite	Vertical	2D (r, z)	Dual permeability in z, homogeneous in r.
Satman et al. (1980), Nie et al. (2019)	Semi-infinite	Vertical	1D (r)	Radial composite regions.
Kuchuk and Habashy (1997)	Semi-infinite, Bounded	Vertical	2D (x, y)	Linear composite regions.
Yaxley (1987), Hosseini (2019), Stewart (2011)	Semi-infinite, Bounded	Vertical	2D (x, y)	Vertical leaky barrier separating two homogeneous regions.
Mavor and Walkup (1986)	Semi-infinite, Bounded	Vertical	0D[a]	Parallel layers, each with its own independent model — no cross-flow in the reservoir.
Bidaux et al. (1992)	Bounded	Vertical, Limited entry, Fractured	0D[a]	Parallel layers, each with its own independent model — cross-flow allowed with restrictions.
Gerard and Horne (1985)	Semi-infinite	Vertical	3D (x, y, z)	Homogeneous medium, with a pinch-out boundary allowed in one direction.
Larsen (1993)	Semi-infinite, Bounded	Vertical, Limited entry	2D (x, y)	Intersecting linear segments, each with its own (homogeneous) properties. Only late-time linear flow is modeled, thus neglecting early-time behavior.
Silva-Lóez et al. (2018)	Semi-infinite	Fractured	1D (x)	Fractured vertical well in a double porosity reservoir. Only bilinear flow is modeled, and pressure can only be calculated along the fracture axis.
Sagawa et al. (2001)	Bounded	Vertical, Horizontal	0D[a]	Sequence of linear segments of different properties along the wellbore axis. Homogeneous in the perpendicular direction.
Shi et al. (2020)	Bounded	Vertical	2D (r, z)	Parallel layers with different external diameters. Flow is 1D (r) within each layer, and no cross-flow is allowed.
Present work	Bounded	Point-source, any[b]	3D (x, y, z)	Block-shaped regions of different properties arbitrarily/irregularly distributed anywhere in the 3D domain, with no restrictions or simplifications to flow.

[a]The resulting expression can only be calculated at the wellbore.

[b]The point-source can be used as a building block for uniform flow solutions in any wellbore geometry — as is illustrated in the present work for the Limited entry vertical well.

When reservoir models are developed for pressure transient analysis, the nature of simplifying assumptions is heavily influenced by the availability of mathematical techniques which enable a solution not dependent on costly numerical simulation. In that context, traditional analytical solution methods in reservoir literature are only able to handle models: for homogeneous — possibly bounded — domains (Larsen, 1985); with heterogeneity regularly distributed throughout the domain, such as dual porosity (Barenblatt et al., 1960; Warren and Root, 1963) or dual permeability (Ehlig-Economides and Ayoub, 1986); for regular composite or coupled systems such as the radial composite (Satman et al., 1980; Nie et al., 2019), linear composite (Kuchuk and Habashy, 1997), partially communicating fault (Yaxley, 1987; Hosseini, 2019) or two-cell compartmentalized (Stewart, 2011) models; for commingled (Mavor and Walkup, 1986) or coupled (Bidaux et al., 1992) multilayered systems; for simplified systems which are, effectively, one or two-dimensional (Gerard and Horne, 1985; Larsen, 1993); neglecting specific flow regimes, such as radial flow in primarily linear systems (Larsen, 1993; Silva-Lóez et al., 2018); or restricting any heterogeneity to one or two conveniently chosen directions (Sagawa et al., 2001; Shi et al., 2020). A summary of the characteristics and capabilities of each of these models — alongside those of the present work — is displayed in Table 1.

Going beyond what is analytically possible and yet avoiding the complexity, accuracy control requirements and computational costs associated with fully numerical simulators is the main reason behind the development of hybrid analytical–numerical methods. In this regard, the Generalized Integral Transform Technique (GITT) (Cotta, 1986, 1990, 1993, 1994) is very appealing in reservoir engineering, since for the pressure diffusivity equation, a given solution can describe all flow regimes of a transient three-dimensional problem, with arbitrary heterogeneities irregularly distributed throughout the domain. With this technique, formal solutions are readily available for various classes of linear and nonlinear diffusion and convection–diffusion problems; however, specific applications might require the implementation of convergence acceleration schemes for the eigenfunction expansions, so that the associated computational cost remains reasonably low for the application's required accuracy.

The purely analytical Classical Integral Transform Technique (CITT) (Koshlyakov, 1936; Mikhailov and Ozisik, 1984), for which the GITT is an extension, has been used before for solving the fully penetrating (Hovanessian, 1961; Couto and Marsili, 2013) and partially penetrating (Rahman and Bentsen, 2000, 2001, 2003) vertical well problems in a homogeneous closed reservoir. The GITT has also been employed with the two-dimensional convection–diffusion problem for the tracer flow in a five-spot pattern (Almeida and Cotta, 1995, 1996), the analysis of one-dimensional oil displacement through water injection in a core plug (Dias et al., 2012) and the two-dimensional energy balance for the transient sandface temperature in flowing wells with commingled production (Deucher et al., 2017). A general GITT formulation was suggested for heterogeneous reservoirs by Couto et al. (2011), following a procedure previously described for heat conduction in heterogeneous solids (Naveira-Cotta et al., 2009), while numerical results were presented later on by Deucher et al. (2016) but only for a one-dimensional heterogeneous medium. None of these previous works were focused on developing solutions for pressure transient analysis,

which means they did not tackle the issue of accurately representing very short transient times at the sandface in a flowing well, where the eigenfunction expansion's rate of convergence is slower.

In this study, the GITT has been applied to Lord Kelvin's point-source (Kelvin, 1884) — a fundamental solution of the heat conduction equation (Carslaw and Jaeger, 1959), which is analogous to the pressure diffusivity equation. Its use in well testing literature goes back to the partial penetration model by Nisle (1958), and it has since then been used extensively to construct analytical solutions for many problems of practical interest using Green's Functions (Gringarten and Ramey, 1973) or the method of sources and sinks (Ozkan and Raghavan, 1991; Raghavan, 1995).

First, the purely analytical CITT is shown to reproduce the other methods' well-known classical solution to the point-source problem in a closed homogeneous reservoir (Gringarten and Ramey, 1973). These expressions are then employed as filters to improve the rate of convergence of the hybrid GITT, which leads to a novel solution to the point-source in a closed heterogeneous domain that is suitable for pressure transient analysis. Finally, the derived expression for the point-source is used in conjunction with the superposition principle to construct a uniform flow solution for a limited entry vertical well, thus demonstrating the usage of the GITT for other well geometries in heterogeneous reservoirs. Synthetic examples are used to show that the obtained solutions are in good agreement with results from the well-established commercial reservoir simulator *Rubis* (KAPPA, 2017).

2. Pressure diffusivity formulation

The pressure diffusion problem for a heterogeneous and anisotropic reservoir V with external closed boundary S may be described by the following equations:

$$\nabla \cdot (\mathbf{K}(\mathbf{x}) \cdot \nabla p(\mathbf{x},t)) - q\mu_f s(\mathbf{x}-\mathbf{x_w}) = \phi\mu_f c_t \frac{\partial p}{\partial t},\ \mathbf{x}\in V,\ t>0, \tag{1}$$

$$\frac{\partial p}{\partial \mathbf{n}} = \nabla p(\mathbf{x},t)\cdot\mathbf{n} = 0,\ \mathbf{x}\in S,\ t>0, \tag{2}$$

$$p(\mathbf{x},0) = p_i,\ \mathbf{x}\in V, \tag{3}$$

where $\mathbf{K}(\mathbf{x})$ is the permeability tensor, $\mathbf{n}$ is the outward-facing normal unit vector to S, and $s(\mathbf{x}-\mathbf{x_w})$ represents the effect of the flow source or sink. Additional assumptions for this formulation include: gravity and capillary effects are negligible; single-phase, isothermal and non-reactive flow; fluid and rock properties do not vary with pressure; fluid is slightly compressible; and Darcy's law holds. An additional assumption in the present work — which is common in reservoir applications — will be that the reservoir is orthotropic with a constant anisotropy ratio:

$$\mathbf{K}(\mathbf{x}) = \begin{pmatrix} k_x & 0 & 0 \\ 0 & k_y & 0 \\ 0 & 0 & k_z \end{pmatrix} k_D(\mathbf{x}) \tag{4}$$

where $k_D(\mathbf{x_D})$ is dimensionless. Eqs. (1)–(3) can then be nondimensionalized as

$$\nabla\cdot\left[k_D(\mathbf{x_D})\nabla p_D(\mathbf{x_D},t_D)\right] + s_D(\mathbf{x_D}-\mathbf{x_{wD}}) = \frac{\partial p_D}{\partial t_D},\ \mathbf{x_D}\in V,\ t_D>0, \tag{5}$$

$$\frac{\partial p_D}{\partial \mathbf{n}} = \nabla p_D(\mathbf{x_D},t_D)\cdot\mathbf{n} = 0,\ \mathbf{x_D}\in S,\ t_D>0, \tag{6}$$

$$p_D(\mathbf{x_D},0) = 0,\ \mathbf{x_D}\in V, \tag{7}$$

with the dimensionless variables

$$x_D = \frac{x}{L}\sqrt{\frac{k}{k_x}},\ y_D = \frac{y}{L}\sqrt{\frac{k}{k_y}},\ z_D = \frac{z}{L}\sqrt{\frac{k}{k_z}}, \tag{8}$$

$$t_D = \frac{\alpha_t k t}{\phi\mu_f c_t L^2}, \tag{9}$$

$$p_D(\mathbf{x},t_D) = \frac{kL}{\alpha_p q\mu_f}\Delta p(\mathbf{x},t), \tag{10}$$

$$s_D(\mathbf{x_D}-\mathbf{x_{wD}}) = L^3 s(\mathbf{x}-\mathbf{x_w}), \tag{11}$$

where $k = \sqrt[3]{k_x k_y k_z}$ and $\Delta p(\mathbf{x},t) = p_i - p(\mathbf{x},t)$. In Eqs. (8)–(11), L is an arbitrary reference length, and α_t and α_p are unit conversion factors. In the standard oilfield unit system, $\alpha_t = 0.000\,263\,74$ and $\alpha_p = 141.2$. In the metric (SI) system, $\alpha_t = 1.0$ and $\alpha_p = 1/2\pi$. In the present work, the metric system was chosen for all numerical examples.

Two different flow source geometries will be considered: the continuous point-source and the limited entry vertical well. For the point-source, the $s(\mathbf{x}-\mathbf{x_w})$ term in Eqs. (1) and (11) can be written as

$$s(\mathbf{x}-\mathbf{x_w}) = \delta(\mathbf{x}-\mathbf{x_w}) = \delta(x-x_w)\delta(y-y_w)\delta(z-z_w), \tag{12}$$

where $\delta(x-x_w)$ is the Dirac delta function. As for the limited entry vertical well:

$$s(\mathbf{x}-\mathbf{x_w}) = \delta(x-x_w)\delta(y-y_w)\frac{1}{h_w}\cdot \cdot\left[H\left(z-z_w+\frac{h_w}{2}\right) - H\left(z-z_w-\frac{h_w}{2}\right)\right], \tag{13}$$

where $H(z-z_w)$ is the Heaviside step function and h_w is the length of the perforated interval. Substituting Eqs. (12) and (13) into Eq. (11), the dimensionless source terms for each geometry become, respectively,

$$s_D(\mathbf{x_D}-\mathbf{x_{wD}}) = \delta_D(\mathbf{x_D}-\mathbf{x_{wD}}) = \delta_D(x_D-x_{wD})\delta_D(y_D-y_{wD})\delta_D(z_D-z_{wD}) \tag{14}$$

and

$$s_D(\mathbf{x_D}-\mathbf{x_{wD}}) = \frac{\delta_D(x_D-x_{wD})\delta_D(y_D-y_{wD})}{h_{wD}}\cdot \cdot\left[H\left(z_D-z_{wD}+\frac{h_{wD}}{2}\right) - H\left(z_D-z_{wD}-\frac{h_{wD}}{2}\right)\right], \tag{15}$$

where $\delta_D = L\delta$ and $h_{wD} = h_w/L$. Both problems are actually particular cases of a general nonlinear convection–diffusion formulation which will be solved with the GITT. Once this generalized solution is available, the particular solutions for each flow source geometry can be obtained by substitution of variables.

3. Generalized formulation and solution

The formal GITT solution for the general nonlinear convection-diffusion problem expressed by Eqs. (16)–(20) for the pressure $p_D(\mathbf{x_D},t_D)$ will be introduced:

$$w(\mathbf{x_D})\frac{\partial p_D}{\partial t_D} + \mathcal{L}\left\{p_D(\mathbf{x_D},t_D)\right\} = g(\mathbf{x_D},t_D,p_D),\ \mathbf{x_D}\in V,\ t_D>0, \tag{16}$$

$$\mathcal{B}\left\{p_D(\mathbf{x_D},t_D)\right\} = \varphi(\mathbf{x_D},t_D,p_D),\ \mathbf{x_D}\in S,\ t_D>0, \tag{17}$$

$$p_D(\mathbf{x_D},0) = f(\mathbf{x_D}),\ \mathbf{x_D}\in V, \tag{18}$$

where the $\mathcal{L}$ and $\mathcal{B}$ operators are defined as

$$\mathcal{L} \equiv -\nabla\cdot\left[k_D(\mathbf{x_D})\nabla(\cdot)\right] + d(\mathbf{x_D})(\cdot), \tag{19}$$

$$\mathcal{B} \equiv \alpha(\mathbf{x_D})(\cdot) + \beta(\mathbf{x_D})k_D(\mathbf{x_D})\frac{\partial(\cdot)}{\partial\mathbf{n}}. \tag{20}$$

The solution procedure for the GITT is thoroughly discussed in other works (Cotta et al., 2018), and will only be summarized here. A convenient analytical filter is first chosen to improve the eigenfunction expansion's convergence rate (Cotta and Mikhailov, 1997):

$$p_D(\mathbf{x_D},t_D) = F_D(\mathbf{x_D},t_D) + p_D^*(\mathbf{x_D},t_D), \tag{21}$$

where $F_D(\mathbf{x_D},t_D)$ is the proposed filter expression. Substituting Eq. (21) into Eqs. (16)–(20) results in

$$w(\mathbf{x_D})\frac{\partial p_D^*}{\partial t_D} + \mathcal{L}\left\{p_D^*(\mathbf{x_D},t_D)\right\} = g^*(\mathbf{x_D},t_D,p_D^*),\ \mathbf{x_D}\in V,\ t_D>0, \tag{22}$$

$$\mathcal{B}\left\{p_D^*(\mathbf{x_D},t_D)\right\} = \varphi^*(\mathbf{x_D},t_D,p_D^*),\ \mathbf{x_D}\in S,\ t_D>0, \tag{23}$$

$$p_D^*(\mathbf{x_D},0) = f^*(\mathbf{x_D}),\ \mathbf{x_D}\in V, \tag{24}$$

where

$$g^*(\mathbf{x_D}, t_D) = g(\mathbf{x_D}, t_D) - \mathcal{L}\{F_D(\mathbf{x_D}, t_D)\} - w(\mathbf{x_D})\frac{\partial F_D}{\partial t_D}, \quad (25)$$

$$\varphi^*(\mathbf{x_D}, t_D) = \varphi(\mathbf{x_D}, t_D, p_D^*) - \mathcal{B}\{F_D(\mathbf{x_D}, t_D)\}, \quad (26)$$

$$f^*(\mathbf{x_D}) = f(\mathbf{x_D}) - F_D(\mathbf{x_D}, 0). \quad (27)$$

Due to the spatially concentrated nature of source terms in reservoir applications, failing to apply a suitable filter will result in slower convergence rates — and thus higher computational cost — for positions close to the well, which is not acceptable for pressure transient analysis since this will be the region where accurate representation of the solution is most critical.

The solution procedure can then be summarized as:

1. proposing an eigenvalue problem to transform the filtered partial differential equation (PDE);
2. solving the transformed filtered problem;
3. solving the eigenvalue problem;
4. reconstructing the original PDE's solution.

It should be noted that, even though the $\mathbf{x_D}$ notation for the position vector would seem to imply Cartesian coordinates, this is by no means a limitation for the GITT. The usage of vector notation is intentional, as all equations in Section 3 remain valid for any orthogonal coordinate system, provided the appropriate expressions are used for the ∇ operator, the domain's weight function $w(\mathbf{x_D})$ and the boundary conditions. The coordinate system to be actually adopted in the solution of the problem is the modeler's choice, based on relative advantages due to the exploration of possible symmetries and/or the representation of boundaries and heterogeneous subregions.

Section 2 explicitly uses Cartesian coordinates, as do the subsequent Sections of the present work, for the purposes of demonstrating the usefulness of the GITT in reservoir applications and providing the aforementioned novel expression for the generalized point-source in arbitrarily heterogeneous media.

3.1. Proposing an eigenvalue problem

Separation of Variables can be applied to the homogeneous version of Eqs. (22)–(24), which leads to an eigenvalue problem carrying the original PDE's spatially variable coefficients:

$$\mathcal{L}\{\psi_i(\mathbf{x_D})\} = \mu_i^2 w(\mathbf{x_D})\psi_i(\mathbf{x_D}), \ \mathbf{x_D} \in V, \quad (28)$$

$$\mathcal{B}\{\psi_i(\mathbf{x_D})\} = 0, \ \mathbf{x_D} \in S. \quad (29)$$

The eigenfunctions' orthogonality property then allows for the following integral transform pair:

$$\overline{p_{Di}^*}(t_D) = \int_V w(\mathbf{x_D})\widetilde{\psi}_i(\mathbf{x_D})p_D^*(\mathbf{x_D}, t_D)dv, \quad \text{(transform)} \quad (30)$$

$$p_D^*(\mathbf{x_D}, t_D) = \sum_{i=1}^{\infty} \overline{p_{Di}^*}(t_D)\widetilde{\psi}_i(\mathbf{x_D}), \quad \text{(inverse)} \quad (31)$$

with normalized eigenfunctions and norms given by

$$\widetilde{\psi}_i(\mathbf{x_D}) = \frac{\psi_i(\mathbf{x_D})}{\sqrt{N_{\psi_i}}}, \quad (32)$$

$$N_{\psi_i} = \int_V w(\mathbf{x_D})\psi_i^2(\mathbf{x_D})dv. \quad (33)$$

3.2. Solving the transformed filtered problem

Operating on Eqs. (22)–(24) with $\int_V \widetilde{\psi}_i(\mathbf{x})(\cdot)dv$ yields the following system for the transformed filtered potentials:

$$\frac{d\overline{p_{Di}^*}}{dt_D} + \mu_i^2\overline{p_{Di}^*}(t_D) = \overline{g_i^*}(t_D, \overline{\mathbf{p}_\mathbf{D}^*}(t_D)), \ t_D > 0, \quad (34)$$

$$\overline{p_{Di}^*}(0) = \overline{f}_i, \quad (35)$$

where

$$\overline{g_i^*}(t_D, \overline{\mathbf{p}_\mathbf{D}^*}(t_D)) = \int_V \widetilde{\psi}_i(\mathbf{x_D})g^*(\mathbf{x_D}, t_D, p_D^*)dv - \\ - \int_S \frac{\varphi^*(\mathbf{x_D}, t_D, p_D^*)\left[k_D(\mathbf{x_D})\frac{\partial\widetilde{\psi}_i}{\partial\mathbf{n}} - \widetilde{\psi}_i(\mathbf{x_D})\right]}{\alpha(\mathbf{x_D}) + \beta(\mathbf{x_D})}ds, \quad (36)$$

$$\overline{f}_i = \int_V w(\mathbf{x_D})\widetilde{\psi}_i(\mathbf{x_D})f(\mathbf{x_D})dv, \quad (37)$$

$$\overline{\mathbf{p}_\mathbf{D}^*}(t_D) = \left\{\overline{p_{D1}^*}(t_D), \overline{p_{D2}^*}(t_D), \ldots\right\}^T. \quad (38)$$

The original PDE in $(\mathbf{x_D}, t_D)$ is then reduced to an infinite coupled system of ordinary differential equations (ODE) in t_D which can be solved numerically with reliable, readily available routines for stiff ODE systems after truncation to a sufficiently large finite order. If $\overline{g_i^*}(t_D, \overline{\mathbf{p}_\mathbf{D}^*}(t_D)) = \overline{g_i^*}(t_D)$, the system becomes uncoupled and admits analytical solution by the method of *integrating factors*:

$$\overline{p_{Di}^*}(t_D) = e^{-\mu_i^2 t_D}\left[\overline{f}_i + \int_0^{t_D} e^{\mu_i^2\tau}\overline{g_i^*}(\tau)d\tau\right]. \quad (39)$$

This is actually the case for the applications proposed in the present work, since they remain purely diffusive and linear problems even in a heterogeneous domain.

3.3. Solving the eigenvalue problem

Assuming the eigenvalue problem in Eqs. (28) and (29) admits no analytical solution, it can still itself be solved by the GITT. For that, a simpler auxiliary eigenvalue problem with a known analytical solution can be proposed:

$$\hat{\mathcal{L}}\{\Omega_j(\mathbf{x_D})\} = \eta_j^2\hat{w}(\mathbf{x_D})\Omega_j(\mathbf{x_D}), \ \mathbf{x_D} \in V, \quad (40)$$

$$\hat{\mathcal{B}}\{\Omega_j(\mathbf{x_D})\} = 0, \ \mathbf{x_D} \in S, \quad (41)$$

where the $\hat{\mathcal{L}}$ and $\hat{\mathcal{B}}$ auxiliary operators are defined as

$$\hat{\mathcal{L}} \equiv -\nabla\cdot\left[\hat{k}_D(\mathbf{x_D})\nabla(\cdot)\right] + \hat{d}(\mathbf{x_D})(\cdot), \quad (42)$$

$$\hat{\mathcal{B}} \equiv \alpha(\mathbf{x_D})(\cdot) + \beta(\mathbf{x_D})\hat{k}_D(\mathbf{x_D})\frac{\partial(\cdot)}{\partial\mathbf{n}}. \quad (43)$$

The auxiliary integral transform pair can then be defined as

$$\overline{\psi}_{ij} = \int_V \hat{w}(\mathbf{x_D})\widetilde{\Omega}_j(\mathbf{x_D})\psi_i(\mathbf{x_D})dv, \quad \text{(transform)} \quad (44)$$

$$\psi_i(\mathbf{x_D}) = \sum_{j=1}^{\infty}\overline{\psi}_{ij}\widetilde{\Omega}_j(\mathbf{x_D}), \quad \text{(inverse)} \quad (45)$$

with normalized auxiliary eigenfunctions and norms

$$\widetilde{\Omega}_j(\mathbf{x_D}) = \frac{\Omega_j(\mathbf{x_D})}{\sqrt{N_{\Omega_j}}}, \quad (46)$$

$$N_{\Omega_j} = \int_V \hat{w}(\mathbf{x_D})\Omega_j^2(\mathbf{x_D})dv. \quad (47)$$

Operating on Eqs. (28) and (29) with $\int_V \widetilde{\Omega}_j(\mathbf{x_D})(\cdot)dv$ yields the following infinite algebraic eigenvalue problem:

$$[(\mathbf{A} + \mathbf{C}) - \mu_i^2\mathbf{B}]\overline{\boldsymbol{\psi}}_i = \mathbf{0}, \quad (48)$$

where the $\mathbf{A}$, $\mathbf{B}$ and $\mathbf{C}$ matrices are given by

$$\mathbf{A} \equiv A_{jk} = -\int_S \zeta_j(\mathbf{x_D})(\hat{\mathcal{B}} - \mathcal{B})\left\{\widetilde{\Omega}_k(\mathbf{x_D})\right\}ds - \\ - \int_V \widetilde{\Omega}_j(\mathbf{x_D})(\hat{\mathcal{L}} - \mathcal{L})\left\{\widetilde{\Omega}_k(\mathbf{x_D})\right\}dv, \quad (49)$$

$$\mathbf{B} \equiv B_{jk} = \int_V \hat{w}(\mathbf{x_D})\widetilde{\Omega}_j(\mathbf{x_D})\widetilde{\Omega}_k(\mathbf{x_D})dv, \quad (50)$$

$$\mathbf{C} \equiv C_{jk} = \eta_j^2\delta_{jk}, \quad (51)$$

where

$$\zeta_j(\mathbf{x_D}) = \frac{\widetilde{\Omega}_j(\mathbf{x_D}) - \hat{k}_D(\mathbf{x_D})\frac{\partial\widetilde{\Omega}_j}{\partial\mathbf{n}}}{\alpha(\mathbf{x_D}) + \beta(\mathbf{x_D})}, \quad (52)$$

and where δ_{jk} is the Kronecker delta. Eq. (48) can then be solved numerically for the eigenvalues μ_i and transformed eigenvectors $\overline{\psi}_i$ after truncation to a sufficiently large finite order, and the results used with the auxiliary inverse formula of Eq. (45) to reconstruct the eigenfunctions $\psi_i(\mathbf{x_D})$.

In multidimensional problems, the eigenvalues should be sorted in order of *increasing* magnitude — which correspond to *decreasing* contribution to the final result — before truncation (Cotta et al., 2018). For homogeneous media this is straightforward, as the eigenvalue problem admits analytical solution. In heterogeneous media, the ordering must be chosen *a priori* as it affects the calculation of the eigenvalues themselves in Eq. (48) through the components of the **A**, **B** and **C** matrices. All numerical calculations in the present work employ a sequence of two complementary reordering criteria:

1. Select the auxiliary eigenvalues η_j in order of increasing magnitude of the main diagonal of $\mathbf{B}^{-1}\mathbf{C}$ — which takes into account the length of the domain, but not its heterogeneity $k_D(\mathbf{x_D})$.
2. Augment the selection with additional elements from the main diagonal of $\mathbf{B}^{-1}\mathbf{A}$, also in order of increasing magnitude — which takes into account the domain's heterogeneity $k_D(\mathbf{x_D})$, but not its base dimensions.

3.4. Reconstructing the original PDE's solution

Once the transformed filtered potentials $\overline{p^*_{Di}}(t_D)$ and the eigenfunctions $\psi_i(\mathbf{x_D})$ have been calculated, the inverse formula in Eq. (31) can be used to reconstruct the filtered pressure $p^*_D(\mathbf{x_D}, t_D)$. Combining this with the proposed filter expression $F_D(\mathbf{x_D}, t_D)$ in Eq. (21) then yields $p_D(\mathbf{x_D}, t_D)$ — the original PDE's solution.

4. Applications

4.1. Point-source in a homogeneous reservoir

The problem for the continuous point-source in a homogeneous reservoir V with external closed boundary S is obtained by substituting Eq. (14) into Eqs. (5)–(7), as well as making $k_D(\mathbf{x_D}) = 1$:

$$\nabla^2 p_D(\mathbf{x_D}, t_D) + \delta_D(\mathbf{x_D} - \mathbf{x_{wD}}) = \frac{\partial p_D}{\partial t_D},\ \mathbf{x_D} \in V,\ t_D > 0, \tag{53}$$

$$\frac{\partial p_D}{\partial \mathbf{n}} = \boldsymbol{\nabla} p_D(\mathbf{x_D}, t_D) \cdot \mathbf{n} = 0,\ \mathbf{x_D} \in S,\ t_D > 0, \tag{54}$$

$$p_D(\mathbf{x_D}, 0) = 0,\ \mathbf{x_D} \in V. \tag{55}$$

The formulation in Eqs. (53)–(55) is well-known in well testing literature, and its solution is usually a two-step process: i) calculate the point-source solution in an infinite domain; ii) apply the *method of images* (Larsen, 1985) to create virtual boundaries in each direction by direct superposition of as many infinite domain solutions as required. By contrast, the present solution through integral transforms calculates the finite domain solution directly. Applying this method to infinite domains is possible, but it requires a different approach because the discrete sequence of eigenvalues becomes a continuous spectrum.

In the case of a linear problem in a homogeneous medium, the summation of the inverse formula in Eq. (31) will simply turn into an integral through a limit operation (Ozisik, 1993). In contrast, if the problem is nonlinear or the medium is heterogeneous, the alternatives would be to: truncate the infinite domain down to a sufficiently large size; propose a change of variables mapping the infinite domain into a finite domain (Almeida and Cotta, 1999); or define a virtual moving boundary (Naveira et al., 2009), analogous to the *boundary layer* concept in fluid mechanics.

Only finite domains will be considered in the present work, which is the mathematical equivalent of truncating a potentially infinite domain down to a sufficiently large size.

4.1.1. Integral transform solution

Applying the procedure in Section 3 to Eqs. (53)–(55) with the variable substitutions $w(\mathbf{x_D}) = 1$, $k_D(\mathbf{x_D}) = 1$, $d(\mathbf{x_D}) = 0$, $\alpha(\mathbf{x_D}) = 0$, $\beta(\mathbf{x_D}) = 1$, $f(\mathbf{x_D}) = 0$, $\varphi(\mathbf{x_D}, t_D, p_D) = 0$, $g(\mathbf{x_D}, t_D, p_D) = \delta_D(\mathbf{x_D} - \mathbf{x_{wD}})$ and $F_D(\mathbf{x_D}, t_D) = 0$ yields the following transformed problem:

$$\frac{d\overline{p_{Di}}}{dt_D} + \eta_i^2 \overline{p_{Di}}(t_D) = \widetilde{\Omega}_i(\mathbf{x_{wD}}),\ t_D > 0, \tag{56}$$

$$\overline{p_{Di}}(0) = 0. \tag{57}$$

For clarity, the μ_i and $\widetilde{\psi}_i(\mathbf{x_D})$ notations, respectively, for the eigenvalues and eigenfunctions, will be reserved for *heterogeneous* media. For *homogeneous* media, the η_i and $\widetilde{\Omega}_i(\mathbf{x_D})$ notations will be preferred. This is the same convention used in Section 3.3 to refer to the *auxiliary* eigenvalue problem which, in the present work, will always be a homogeneous version of the eigenvalue problem proposed for the original heterogeneous reservoir.

As the ODE system of Eqs. (56) and (57) is uncoupled, its analytical solution is found by direct application of Eq. (39) (the zeroth index $i = 0$ refers to the null eigenvalue $\eta_0 = 0$):

$$\overline{p_{Di}}(t_D) = \begin{cases} \widetilde{\Omega}_0(\mathbf{x_{wD}}) t_D, & i = 0, \\ \dfrac{\widetilde{\Omega}_i(\mathbf{x_{wD}})}{\eta_i^2}\left(1 - e^{-\eta_i^2 t_D}\right), & i \geq 1. \end{cases} \tag{58}$$

The proposed eigenvalue problem is

$$\nabla^2 \Omega_i(\mathbf{x_D}) + \eta_i^2 \Omega_i(\mathbf{x_D}) = 0,\ \mathbf{x_D} \in V, \tag{59}$$

$$\frac{\partial \Omega_i}{\partial \mathbf{n}} = 0,\ \mathbf{x_D} \in S, \tag{60}$$

which is obtained from Eqs. (40)–(43) by substituting $\hat{w}(\mathbf{x_D}) = 1$, $\hat{k}_D(\mathbf{x_D}) = 1$, $\hat{d}(\mathbf{x_D}) = 0$, $\alpha(\mathbf{x_D}) = 0$ and $\beta(\mathbf{x_D}) = 1$. Eq. (59) is recognizable as the multidimensional *Helmholtz Equation*, whose solution can be obtained by Separation of Variables. In three-dimensional Cartesian coordinates this is given by

$$\widetilde{\Omega}_i(\mathbf{x_D}) = \widetilde{X}_{i_x}(x_D)\widetilde{Y}_{i_y}(y_D)\widetilde{Z}_{i_z}(z_D), \tag{61}$$

$$\eta_i^2 = \lambda_{i_x}^2 + \gamma_{i_y}^2 + \nu_{i_z}^2, \tag{62}$$

where $\widetilde{\mathcal{X}}_k(\upsilon_D) \in \left\{\widetilde{X}_{i_x}(x_D), \widetilde{Y}_{i_y}(y_D), \widetilde{Z}_{i_z}(z_D)\right\}$ are the one-dimensional eigenfunctions given by

$$\mathcal{X}_k(\upsilon_D) = \cos\left(\rho_k \upsilon_D\right), \tag{63}$$

$$\rho_k = \frac{k\pi}{L_{\upsilon D}}, \tag{64}$$

$$N_{\mathcal{X}_k} = \begin{cases} L_{\upsilon D}, & k = 0, \\ \frac{L_{\upsilon D}}{2}, & k \geq 1, \end{cases} \tag{65}$$

$$\widetilde{\mathcal{X}}_k(\upsilon_D) = \frac{\mathcal{X}_k(\upsilon_D)}{\sqrt{N_{\mathcal{X}_k}}}, \tag{66}$$

where $\rho_k \in \left\{\lambda_{i_x}, \gamma_{i_y}, \nu_{i_z}\right\}$, $\upsilon_D \in \left\{x_D, y_D, z_D\right\}$ and $k \in \{0, 1, 2, \ldots\}$. Substituting Eqs. (58) and (61)–(66) into the inversion formula of Eq. (31) yields the point-source solution by integral transform:

$$p_D(\mathbf{x_D}, t_D) = \widetilde{\Omega}_0(\mathbf{x_{wD}})\widetilde{\Omega}_0(\mathbf{x_D}) t_D + \sum_{i=1}^{\infty} \frac{\widetilde{\Omega}_i(\mathbf{x_{wD}})\widetilde{\Omega}_i(\mathbf{x_D})}{\eta_i^2}\left(1 - e^{-\eta_i^2 t_D}\right). \tag{67}$$

And, taking the derivative with respect to time:

$$\frac{\partial p_D}{\partial t_D} = \sum_{i=0}^{\infty} \widetilde{\Omega}_i(\mathbf{x_{wD}})\widetilde{\Omega}_i(\mathbf{x_D}) e^{-\eta_i^2 t_D}. \tag{68}$$

For well testing applications, solution accuracy is most needed at the well, which happens to be the location where Eqs. (67) and (68) will be the slowest to converge, due to the influence of the Dirac delta source term. The $1/\eta_i^2$ term in Eq. (67), in particular, does not have exponential decay and will never perform adequately for such applications. Nevertheless, these expressions are formally correct, and

Section 4.1.2 will show how appropriate algebraic manipulation may be used to improve their computational performance during the early transient period.

4.1.2. Relationship between the method of images and integral transform solutions

As the CITT solution of Eq. (67) and the method of images solution of Eq. (A.1) both satisfy the problem in Eqs. (53)–(55), it should be possible to demonstrate their mathematical equivalence. Starting from the time derivative of the CITT solution in Eq. (68), substituting the eigenvalue problem solution of Eqs. (61)–(66), rewriting the single summation as a triple summation and grouping together the terms in each orthogonal direction yields

$$\begin{aligned}\frac{\partial p_D}{\partial t_D} = &\left(\sum_{m=0}^{\infty}\frac{1}{N_{X_m}}\cos\left(\lambda_m x_{wD}\right)\cos\left(\lambda_m x_D\right)e^{-\lambda_m^2 t_D}\right)\cdot\\ &\cdot\left(\sum_{n=0}^{\infty}\frac{1}{N_{Y_n}}\cos\left(\gamma_n y_{wD}\right)\cos\left(\gamma_n y_D\right)e^{-\gamma_n^2 t_D}\right)\cdot\\ &\cdot\left(\sum_{p=0}^{\infty}\frac{1}{N_{Z_p}}\cos\left(\nu_p z_{wD}\right)\cos\left(\nu_p z_D\right)e^{-\nu_p^2 t_D}\right)\end{aligned} \tag{69}$$

As the three terms in Eq. (69) are analogous, any algebraic manipulations on one term can be readily extended to the remaining two. Applying the trigonometric identities for the sum and subtraction of cosines, the term in x can be written as

$$\begin{aligned}&\sum_{m=0}^{\infty}\frac{1}{N_{X_m}}\cos\left(\lambda_m x_{wD}\right)\cos\left(\lambda_m x_D\right)e^{-\lambda_m^2 t_D}\\ &\quad=\sum_{k=1}^{2}\frac{1}{2L_{xD}}\left[1+2\sum_{m=1}^{\infty}\exp\left(-\frac{m^2\pi^2 t_D}{L_{xD}^2}\right)\cdot\right.\\ &\qquad\left.\cdot\cos\left(m\pi\frac{x_D+(-1)^k x_{wD}}{L_{xD}}\right)\right]\end{aligned} \tag{70}$$

Except for the change in notation, each term on the right-hand side of Eq. (70) corresponds exactly to the right-hand side of the *Poisson summation* formula (Raghavan, 1995):

$$\begin{aligned}&\sum_{n=-\infty}^{+\infty}\exp\left[-\frac{(\xi-2n\xi_e)^2}{4t}\right]\\ &\quad=\frac{\sqrt{\pi t}}{\xi_e}\left[1+2\sum_{n=1}^{\infty}\exp\left(-\frac{n^2\pi^2 t}{\xi_e^2}\right)\cos\left(n\pi\frac{\xi}{\xi_e}\right)\right]\end{aligned} \tag{71}$$

As such, rewriting Eq. (70) with Eq. (71) yields

$$\begin{aligned}&\sum_{m=0}^{\infty}\frac{1}{N_{X_m}}\cos\left(\lambda_m x_{wD}\right)\cos\left(\lambda_m x_D\right)e^{-\lambda_m^2 t_D}\\ &\quad=\frac{1}{\left(4\pi t_D\right)^{3/2}}\sum_{n=-\infty}^{+\infty}\sum_{k=1}^{2}\exp\left[-\frac{(x_D+(-1)^k x_{wD})^2}{4t_D}\right]\end{aligned} \tag{72}$$

Extending the manipulation in Eq. (72) to the y and z terms, Eq. (69) can be rewritten as

$$\frac{\partial p_D}{\partial t_D}=\frac{1}{(4\pi t_D)^{3/2}}\sum_{m=-\infty}^{+\infty}\sum_{n=-\infty}^{+\infty}\sum_{p=-\infty}^{+\infty}\sum_{k=1}^{2}\sum_{j=1}^{2}\sum_{i=1}^{2}\exp\left(-\frac{R_{Dkm,jn,ip}^2}{4t_D}\right), \tag{73}$$

where $R_{Dkm,jn,ip}$ is given by Eq. (A.2). Eq. (73) is identical to Eq. (A.3), which is the time derivative of the classical method of images solution. Therefore, both methods produce, in fact, alternative forms of the same solution.

It should be noted, however, that these alternative forms are known to display distinct convergence characteristics (Raghavan, 1995): the exponential form of Eqs. (A.1) and (A.3) converges rapidly in *early times*, when $t_D \leq {}^{L_{vD}^2}/_{\pi}$ in each orthogonal direction v; whereas the integral transform form of Eqs. (67) and (68) converges rapidly in the *late time*, when $t_D \geq {}^{L_{vD}^2}/_{\pi}$. Using the numerical parameters of Table 2 in Section 5.1, these reference values for t_D would be 8.2 days (197 hours) in the x and y directions, and 3.1 hours in the z direction. This improved convergence behavior in the early-time region, which is of main interest to well testing applications, is the reason for which the exponential form will be preferred for numerical calculations throughout the present work.

4.2. Point-source in a heterogeneous reservoir

The problem for the continuous point-source in a heterogeneous reservoir V with external closed boundary S is obtained by substituting Eq. (14) into Eqs. (5)–(7):

$$\nabla\cdot\left[k_D(\mathbf{x_D})\nabla p_D(\mathbf{x_D},t_D)\right]+\delta_D(\mathbf{x_D}-\mathbf{x_{wD}})=\frac{\partial p_D}{\partial t_D},\ \mathbf{x_D}\in V,\ t_D>0, \tag{74}$$

$$\frac{\partial p_D}{\partial \mathbf{n}}=\nabla p_D(\mathbf{x_D},t_D)\cdot\mathbf{n}=0,\ \mathbf{x_D}\in S,\ t_D>0, \tag{75}$$

$$p_D(\mathbf{x_D},0)=0,\ \mathbf{x_D}\in V, \tag{76}$$

The point-source solution in Eq. (67) for a homogeneous reservoir — or its exponential equivalent in Eq. (A.4) — accounts directly for the effects of the Dirac delta during the early transient period in this PDE, and does not create any additional nonhomogeneities in the initial or boundary conditions. For these reasons, it is likely a good choice for the filter expression $F_D(\mathbf{x_D},t_D)$, to improve the convergence rate of the eigenfunction expansion for the heterogeneous reservoir. Since the filter expression represents a homogeneous domain, a single permeability value must be chosen to remove as much information as possible from the heterogeneous PDE's source term, and the most natural candidate is the permeability at the Dirac delta's position:

$$k_D(\mathbf{x_D})\Big|_{\mathbf{x_D}=\mathbf{x_{wD}}}=k_D(\mathbf{x_{wD}})\equiv k_{wD} \tag{77}$$

Rewriting Eqs. (53)–(55) for the filter $F_D(\mathbf{x_D},t_D)$ with $k_D(\mathbf{x_D})=k_{wD}$ instead of $k_D(\mathbf{x_D})=1$ yields

$$k_{wD}\nabla^2 F_D(\mathbf{x_D},t_D)+\delta_D(\mathbf{x_D}-\mathbf{x_{wD}})=\frac{\partial F_D}{\partial t_D},\ \mathbf{x_D}\in V,\ t_D>0, \tag{78}$$

$$\frac{\partial F_D}{\partial \mathbf{n}}=\nabla F_D(\mathbf{x_D},t_D)\cdot\mathbf{n}=0,\ \mathbf{x_D}\in S,\ t_D>0, \tag{79}$$

$$F_D(\mathbf{x_D},0)=0,\ \mathbf{x_D}\in V. \tag{80}$$

whose solution and time derivative can be adapted from Eqs. (67) and (68) by replacing k_x, k_y and k_z with, respectively, $k_x k_{wD}$, $k_y k_{wD}$ and $k_z k_{wD}$ in the definition of the dimensionless numbers in Eqs. (8)–(10):

$$\begin{aligned}F_D(\mathbf{x_D},t_D)=&\ \widetilde{\Omega}_0(\mathbf{x_{wD}})\widetilde{\Omega}_0(\mathbf{x_D})t_D+\\ &+\sum_{j=1}^{\infty}\frac{\widetilde{\Omega}_j(\mathbf{x_{wD}})\widetilde{\Omega}_j(\mathbf{x_D})}{k_{wD}\eta_j^2}\left(1-e^{-k_{wD}\eta_j^2 t_D}\right),\end{aligned} \tag{81}$$

$$\frac{\partial F_D}{\partial t_D}=\sum_{j=0}^{\infty}\widetilde{\Omega}_j(\mathbf{x_{wD}})\widetilde{\Omega}_j(\mathbf{x_D})e^{-k_{wD}\eta_j^2 t_D}. \tag{82}$$

Or, alternatively, in the exponential form:

$$F_D(\mathbf{x_D},t_D)=\sum_{j=0}^{\infty}\frac{1}{4\pi k_{wD}R_{Dj}(\mathbf{x_D})}\operatorname{erfc}\left(\frac{R_{Dj}(\mathbf{x_D})}{2\sqrt{k_{wD}t_D}}\right), \tag{83}$$

$$\frac{\partial F_D}{\partial t_D}=\sum_{j=0}^{\infty}\frac{1}{(4\pi k_{wD}t_D)^{3/2}}\exp\left(-\frac{{R_D}_j^2(\mathbf{x_D})}{4k_{wD}t_D}\right), \tag{84}$$

which correspond to Eqs. (A.4) and (A.5) when $k_{wD}=1$.

Applying the GITT procedure to Eqs. (74)–(76) with the variable substitutions $w(\mathbf{x_D})=1$, $d(\mathbf{x_D})=0$, $\alpha(\mathbf{x_D})=0$, $\beta(\mathbf{x_D})={}^1/_{k_D}(\mathbf{x_D})$, $f(\mathbf{x_D})=0$, $\varphi(\mathbf{x_D},t_D,p_D)=0$, $g(\mathbf{x_D},t_D,p_D)=\delta_D(\mathbf{x_D}-\mathbf{x_{wD}})$ and $F_D(\mathbf{x_D},t_D)$ from Eq. (81) yields the following filtered problem:

$$\nabla\cdot\left[k_D(\mathbf{x_D})\nabla p_D^*(\mathbf{x_D},t_D)\right]+g^*(\mathbf{x_D},t_D)=\frac{\partial p_D^*}{\partial t_D},\ \mathbf{x_D}\in V,\ t_D>0, \tag{85}$$

$$\frac{\partial p_D^*}{\partial \mathbf{n}}=\nabla p_D^*(\mathbf{x_D},t_D)\cdot\mathbf{n}=0,\ \mathbf{x_D}\in S,\ t_D>0, \tag{86}$$

$$p_D^*(\mathbf{x_D}, 0) = 0, \ \mathbf{x_D} \in V, \tag{87}$$

where

$$g^*(\mathbf{x_D}, t_D) = \nabla \cdot \left[(k_D(\mathbf{x_D}) - k_{wD})\nabla F_D(\mathbf{x_D}, t_D)\right] \tag{88}$$

It is clear in Eq. (88) that the spatially concentrated Dirac delta source term was replaced by a continuous, distributed function. This change is expected to have a positive impact on the solution's rate of convergence, especially for positions close to the point-source. It should be noted that by choosing k_{wD} as the characteristic coefficient, the filtered source term becomes zero at the actual source's original position.

The solution $p_D(\mathbf{x_D}, t_D)$ to Eqs. (74)–(76) will be obtained by substituting Eq. (31) into Eq. (21):

$$p_D(\mathbf{x_D}, t_D) = F_D(\mathbf{x_D}, t_D) + \sum_{i=0}^{\infty} \overline{p_{Di}^*}(t_D)\widetilde{\psi}_i(\mathbf{x_D}), \tag{89}$$

with time derivative given by

$$\frac{\partial p_D}{\partial t_D} = \frac{\partial F_D}{\partial t_D} + \sum_{i=0}^{\infty} \frac{d\overline{p_{Di}^*}}{dt_D}\widetilde{\psi}_i(\mathbf{x_D}). \tag{90}$$

While the filter expressions $F_D(\mathbf{x_D}, t_D)$ and $\frac{\partial F_D}{\partial t_D}$ are shown in Eqs. (81)–(84), the transformed potentials $\overline{p_{Di}^*}(t_D)$, their derivatives $\frac{d\overline{p_{Di}^*}}{dt_D}$ and the eigenfunctions $\widetilde{\psi}_i(\mathbf{x_D})$ remain to be calculated.

4.2.1. Solving the eigenvalue problem

The eigenvalue problem is defined in Eqs. (28) and (29). As it has no analytical solution for a general $k_D = k_D(\mathbf{x_D})$, the GITT itself can be applied to provide a solution. The variable substitutions $\hat{w}(\mathbf{x_D}) = 1$, $\hat{d}(\mathbf{x_D}) = 0$ and $\hat{k}_D(\mathbf{x_D}) = k_{wD}$ yield the auxiliary eigenvalue problem

$$k_{wD}\nabla^2\widetilde{\Omega}_m(\mathbf{x_D}) + \eta_m^2\widetilde{\Omega}_m(\mathbf{x_D}) = 0, \ \mathbf{x_D} \in V, \tag{91}$$

$$\frac{\partial\widetilde{\Omega}_m}{\partial\mathbf{n}} = 0, \ \mathbf{x_D} \in S, \tag{92}$$

with its corresponding transform and inverse formulae: transform:

$$\overline{\psi}_{im} = \int_V \psi_i(\mathbf{x_D})\widetilde{\Omega}_m(\mathbf{x_D})dv, \tag{93}$$

inverse:

$$\psi_i(\mathbf{x_D}) = \sum_{m=0}^{\infty} \overline{\psi}_{im}\widetilde{\Omega}_m(\mathbf{x_D}), \tag{94}$$

The resulting algebraic eigenvalue problem is then obtained from Eqs. (48)–(51):

$$(\mathbf{A} - \mu_i^2\mathbf{I})\overline{\boldsymbol{\psi}}_i = \mathbf{0}, \tag{95}$$

where

$$\mathbf{A} \equiv A_{jk} = \int_V k_D(\mathbf{x_D})\nabla\widetilde{\Omega}_j(\mathbf{x_D}) \cdot \nabla\widetilde{\Omega}_k(\mathbf{x_D})dv, \tag{96}$$

and $\mathbf{I}$ is the identity matrix. For particular forms of the function $k_D(\mathbf{x_D})$, the integration of A_{jk} may be carried out analytically. For more complicated forms of $k_D(\mathbf{x_D})$, numeric integration might not be the most appropriate alternative because the integration of the eigenfunctions $\widetilde{\Omega}_j(\mathbf{x_D})$, which become highly oscillatory as j increases, can have a high associated computational cost. In contrast, $k_D(\mathbf{x_D})$ is generally a well-behaved function in most practical applications. A semi-analytical integration technique may be employed in these cases (Cotta and Mikhailov, 2005; Cotta et al., 2015), where the integration domain is partitioned into disjoint sub-domains in which the $k_D(\mathbf{x_D})$ function can be approximated and removed from the integral.

Using this concept, the heterogeneous domain will be constructed over a starting homogeneous domain V from N disjoint rectangular blocks inside which the $k_D(\mathbf{x_D})$ function is constant, as illustrated in Fig. 1. It should be noted that the GITT is certainly not limited to these kinds of geometries, having been previously applied in heat transfer to more irregular forms (Knupp et al., 2015; Almeida et al., 2020). That said, the block geometry is simpler to construct and can still approximate many cases of practical interest. The integral in Eq. (96) for V can then be split into separate integrals for each rectangular block, thus removing $k_D(\mathbf{xD})$ from the integrand:

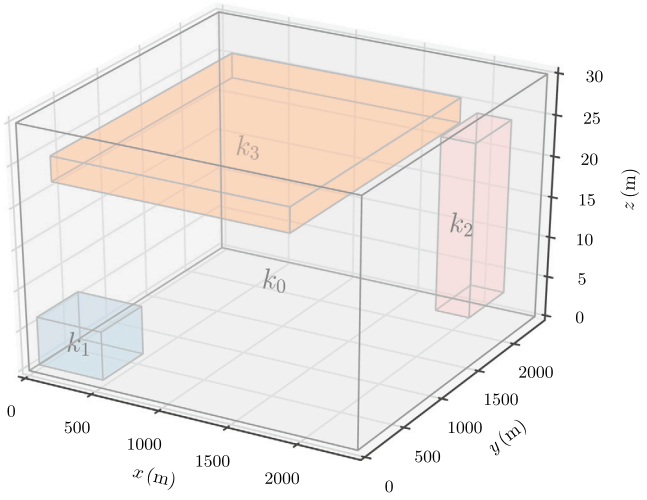

Fig. 1. Heterogeneous domain constructed over a starting homogeneous domain V from N disjoint rectangular blocks inside which the $k_D(\mathbf{x_D})$ function is constant.

$$A_{jk} = k_{wD}I_{jk}(V) - \sum_{n=1}^{N}(k_{wD} - k_{Dn})I_{jk}(V_n), \tag{97}$$

where

$$I_{jk}(V_n) = \int_{V_n} \nabla\widetilde{\Omega}_j(\mathbf{x_D}) \cdot \nabla\widetilde{\Omega}_k(\mathbf{x_D})dv. \tag{98}$$

For the whole domain V, the expression for $I_{jk}(V)$ can be further simplified through the application of Green's first identity, which yields

$$I_{jk}(V) = \frac{\eta_k^2}{k_{wD}}\delta_{jk}. \tag{99}$$

For the rectangular blocks V_n, it should be noted that the auxiliary eigenvalue problem for $\widetilde{\Omega}_m(\mathbf{x_D})$ in Eqs. (91) and (92) is identical to Eqs. (59) and (60) for the homogeneous point-source after the change of variables $\eta_m = \eta'_m\sqrt{k_{wD}}$. Therefore, its solution is given by Eqs. (61)–(66) with the same change of variables. The remaining integrals $I_{jk}(V_n)$ can then be simplified from Eq. (98) as

$$I_{jk}(V_n) = I_{X'}I_YI_Z + I_XI_{Y'}I_Z + I_XI_YI_{Z'}, \tag{100}$$

with the various one-dimensional integrals given by

$$I_{\mathcal{X}} = \int \widetilde{\mathcal{X}}_{j_v}(v_D)\widetilde{\mathcal{X}}_{k_v}(v_D)dv_D = \begin{cases} \text{if } \rho_{j_v} \neq \rho_{k_v}\text{:} \\ \dfrac{1}{2\sqrt{N_{\mathcal{X}_{j_v}}N_{\mathcal{X}_{k_v}}}}\left[\dfrac{\sin\left[(\rho_{j_v} - \rho_{k_v})v_D\right]}{\rho_{j_v} - \rho_{k_v}} + \dfrac{\sin\left[(\rho_{j_v} + \rho_{k_v})v_D\right]}{\rho_{j_v} + \rho_{k_v}}\right] \\ \text{if } \rho_{j_v} = \rho_{k_v} \neq 0\text{:} \\ \dfrac{1}{2N_{\mathcal{X}_{j_v}}}\left[v_D + \dfrac{\sin(2\rho_{j_v}v_D)}{2\rho_{j_v}}\right] \\ \text{if } \rho_{j_v} = \rho_{k_v} = 0\text{:} \\ \dfrac{v_D}{N_{\mathcal{X}_{j_v}}} \end{cases} \tag{101}$$

$$I_{\mathcal{X}'} = \int \widetilde{\mathcal{X}}'_{j_v}(v_D)\widetilde{\mathcal{X}}'_{k_v}(v_D)dv_D$$
$$= \begin{cases} \text{if } \rho_{j_v} \neq \rho_{k_v}: \\ \dfrac{\rho_{j_v}\rho_{k_v}}{2\sqrt{N_{\mathcal{X}_{j_v}} N_{\mathcal{X}_{k_v}}}}\left[\dfrac{\sin\left[(\rho_{j_v}-\rho_{k_v})v_D\right]}{\rho_{j_v}-\rho_{k_v}} - \dfrac{\sin\left[(\rho_{j_v}+\rho_{k_v})v_D\right]}{\rho_{j_v}+\rho_{k_v}}\right] \\ \text{if } \rho_{j_v} = \rho_{k_v}: \\ \dfrac{\rho_{j_v}}{4N_{\mathcal{X}_{j_v}}}\left[2\rho_{j_v}v_D - \sin\left(2\rho_{j_v}v_D\right)\right] \end{cases} \tag{102}$$

with the same conventions adopted in Eqs. (63)–(66). Substituting Eqs. (99)–(102) into Eqs. (97) and (98), all elements in the **A** matrix of the algebraic eigenvalue problem of Eqs. (95) and (96) can be calculated. The solution to this problem, using a sufficiently large truncation order, yields the eigenvalues μ_i and their associated transformed eigenvectors $\overline{\psi}_{ij}$. The inverse formula in Eq. (94) can then be used to reconstruct the eigenfunctions $\psi_i(\mathbf{x_D})$ of the original heterogeneous eigenvalue problem. As the respective orthogonality properties of both $\psi_i(\mathbf{x_D})$ and $\Omega_m(\mathbf{x_D})$ share the same weighting function $w(\mathbf{x_D}) = \hat{w}(\mathbf{x_D}) = 1$, substituting Eq. (45) into Eq. (33) allows for the eigenfunctions' norm to be conveniently simplified to

$$N_{\psi_i} = \sum_{j=1}^{\infty} \overline{\psi}_{ij}^2 \tag{103}$$

4.2.2. Calculating the transformed potentials

The GITT procedure yields the following problem for the transformed potentials:

$$\frac{d\overline{p^*_{Di}}}{dt_D} + \mu_i^2\overline{p^*_{Di}}(t_D) = \overline{g^*_i}(t_D), \tag{104}$$
$$\overline{p^*_{Di}}(0) = 0, \tag{105}$$

where

$$\overline{g^*_i}(t_D) = \int_V \widetilde{\psi}_i(\mathbf{x_D})g^*(\mathbf{x_D}, t_D)dv. \tag{106}$$

Substituting Eq. (88) into Eq. (106) and simplifying through the use of Green's second identity yields

$$\overline{g^*_i}(t_D) = \frac{1}{\sqrt{N_{\psi_i}}}\sum_{m=0}^{\infty}\overline{\psi}_{im}\left(\eta_m^2 - \mu_i^2\right)\int_V F_D(\mathbf{x_D}, t_D)\widetilde{\Omega}_m(\mathbf{x_D})dv, \tag{107}$$

where the eigenfunctions $\widetilde{\psi}_i(\mathbf{x_D})$ have been transformed by the auxiliary eigenfunctions $\widetilde{\Omega}_m(\mathbf{x_D})$, according to the transform and inverse formulae of Eqs. (93) and (94). By substituting Eq. (81) into Eq. (107), the final expression for the transformed source $\overline{g^*_i}(t_D)$ is obtained:

$$\overline{g^*_i}(t_D) = \frac{1}{\sqrt{N_{\psi_i}}}\left[-\overline{\psi}_{i0}\mu_i^2\widetilde{\Omega}_0(\mathbf{x_{wD}})t_D + \right.$$
$$\left. + \sum_{m=1}^{\infty}\overline{\psi}_{im}\left(\frac{\eta_m^2-\mu_i^2}{k_{wD}\eta_m^2}\right)\widetilde{\Omega}_m(\mathbf{x_{wD}})\left(1 - e^{-k_{wD}\eta_m^2 t_D}\right)\right]. \tag{108}$$

With Eq. (108), the linear ODE system of Eqs. (104) and (105) can now be solved. It is uncoupled, therefore its analytical solution is given by Eq. (39):

$$\overline{p^*_{Di}}(t_D) = \int_0^{t_D} e^{-\mu_i^2(t_D-\tau)}\overline{g^*_i}(\tau)d\tau$$
$$= \begin{cases} \text{if } i = 0: \\ \dfrac{1}{\sqrt{N_{\psi_0}}}\sum_{m=1}^{\infty}\overline{\psi}_{0m}\dfrac{\widetilde{\Omega}_m(\mathbf{x_{wD}})}{k_{wD}}T_{0m}(t_D), \\ \text{if } i \geq 1: \\ \dfrac{1}{\sqrt{N_{\psi_i}}}\left[-\overline{\psi}_{i0}\widetilde{\Omega}_0(\mathbf{x_{wD}})T_{i0}(t_D) + \right. \\ \left. + \sum_{m=1}^{\infty}\overline{\psi}_{im}\dfrac{\widetilde{\Omega}_m(\mathbf{x_{wD}})}{k_{wD}}T_{im}(t_D)\right] \end{cases} \tag{109}$$

where

$$T_{im}(t_D) = \begin{cases} \text{if } i = 0,\ m \geq 1: \\ t_D - \dfrac{1}{k_{wD}\eta_m^2}\left(1 - e^{-k_{wD}\eta_m^2 t_D}\right) \\ \text{if } i \geq 1,\ m = 0: \\ t_D - \dfrac{1}{\mu_i^2}\left(1 - e^{-\mu_i^2 t_D}\right) \\ \text{if } i \geq 1,\ m \geq 1: \\ \left(\dfrac{1}{\mu_i^2} - \dfrac{1}{\eta_m^2}\right)\left(1 - e^{-\mu_i^2 t_D}\right) - \\ -\dfrac{1}{\eta_m^2}\left(\dfrac{\eta_m^2-\mu_i^2}{k_{wD}\eta_m^2-\mu_i^2}\right)\left[e^{-\mu_i^2 t_D} - e^{-k_{wD}\eta_m^2 t_D}\right] \end{cases} \tag{110}$$

The time derivative can then be directly obtained from Eq. (109):

$$\frac{d\overline{p^*_{Di}}}{dt_D} = \begin{cases} \text{if } i = 0: \\ \dfrac{1}{\sqrt{N_{\psi_0}}}\sum_{m=1}^{\infty}\overline{\psi}_{0m}\dfrac{\widetilde{\Omega}_m(\mathbf{x_{wD}})}{k_{wD}}\dfrac{dT_{0m}}{dt_D} \\ \text{if } i \geq 1: \\ \dfrac{1}{\sqrt{N_{\psi_i}}}\left[-\overline{\psi}_{i0}\widetilde{\Omega}_0(\mathbf{x_{wD}})\dfrac{dT_{i0}}{dt_D} + \right. \\ \left. + \sum_{m=1}^{\infty}\overline{\psi}_{im}\dfrac{\widetilde{\Omega}_m(\mathbf{x_{wD}})}{k_{wD}}\dfrac{dT_{im}}{dt_D}\right] \end{cases} \tag{111}$$

where

$$\frac{dT_{im}}{dt_D} = \begin{cases} \text{if } i = 0,\ m \geq 1: \\ 1 - e^{-k_{wD}\eta_m^2 t_D} \\ \text{if } i \geq 1,\ m = 0: \\ 1 - e^{-\mu_i^2 t_D} \\ \text{if } i \geq 1,\ m \geq 1: \\ \left(1 - \dfrac{\mu_i^2}{\eta_m^2}\right)e^{-\mu_i^2 t_D} - \left(\dfrac{\eta_m^2-\mu_i^2}{k_{wD}\eta_m^2-\mu_i^2}\right)\cdot \\ \cdot\left[k_{wD}e^{-k_{wD}\eta_m^2 t_D} - \dfrac{\mu_i^2}{\eta_m^2}e^{-\mu_i^2 t_D}\right] \end{cases} \tag{112}$$

4.3. Limited entry vertical well in a heterogeneous reservoir

The problem for a limited entry vertical well in a heterogeneous reservoir V with external closed boundary S is obtained by substituting Eq. (15) into Eqs. (5)–(7):

$$\nabla\cdot\left[k_D(\mathbf{x_D})\nabla p_D(\mathbf{x_D}, t_D)\right] + s_D(\mathbf{x_D} - \mathbf{x_{wD}}) = \frac{\partial p_D}{\partial t_D},\ \mathbf{x_D} \in V,\ t_D > 0, \tag{113}$$
$$\frac{\partial p_D}{\partial \mathbf{n}} = \nabla p_D(\mathbf{x_D}, t_D)\cdot\mathbf{n} = 0,\ \mathbf{x_D} \in S,\ t_D > 0, \tag{114}$$
$$p_D(\mathbf{x_D}, 0) = 0,\ \mathbf{x_D} \in V. \tag{115}$$

Eqs. (113)–(115) describe a uniform flow formulation. Since the problems for $p_D(\mathbf{x_D}, t_D)$ in the limited entry well and $p_{Dps}(\mathbf{x_D}, t_D)$ in the

point-source are both linear, it is convenient to apply the superposition principle:

$$p_D(\mathbf{x_D}, t_D) = \frac{1}{\mathcal{S}} \int_{\mathcal{S}} p_{D_{ps}}(\mathbf{x_D}, t_D) ds, \tag{116}$$

where $\mathcal{S}$ represents the length, area or volume of the source. With Eq. (116), the GITT solution for the point-source demonstrated in the present work can be used as a building block to obtain linear uniform flow solutions for any well geometry in heterogeneous reservoirs. If necessary, these uniform flow solutions could then be used as building blocks themselves, to obtain infinite conductivity solutions either through traditional procedures (Gringarten and Ramey, 1973) or more recently proposed methods (Biryukov and Kuchuk, 2012b). Alternatively, if the problem under consideration was nonlinear, the generalized solution in Section 3 could still be applied directly — in this case, restricting the usage of the superposition principle for building a convenient linear filter expression $F_D(\mathbf{x_D}, t_D)$ from the simpler homogeneous point-source.

Substituting Eq. (89) for $p_{D_{ps}}(\mathbf{x_D}, t_D)$ into Eq. (116), where $\mathcal{S}$ stands for the length of the perforated interval from $z_D = z_{w_D} - h_{wD}/2$ to $z_D = z_{w_D} + h_{wD}/2$, yields

$$p_D(\mathbf{x_D}, t_D) = F_D(\mathbf{x_D}, t_D) + \sum_{i=0}^{\infty} \overline{p^*_{Di}}(t_D) \widetilde{\psi}_i(\mathbf{x_D}), \tag{117}$$

where

$$F_D(\mathbf{x_D}, t_D) = \frac{1}{h_{wD}} \int_{z_{wD}-h_{wD}/2}^{z_{wD}+h_{wD}/2} F_{D_{ps}}(\mathbf{x_D}, t_D) dz'_{wD}, \tag{118}$$

$$\overline{p^*_{Di}}(t_D) = \frac{1}{h_{wD}} \int_{z_{wD}-h_{wD}/2}^{z_{wD}+h_{wD}/2} \left[\overline{p^*_{Di}}\right]_{ps}(\mathbf{x_D}, t_D) dz'_{wD}, \tag{119}$$

with the corresponding time derivative

$$\frac{\partial p_D}{\partial t_D} = \frac{\partial F_D}{\partial t_D} + \sum_{i=0}^{\infty} \frac{d\overline{p^*_{Di}}}{dt_D} \widetilde{\psi}_i(\mathbf{x_D}). \tag{120}$$

The $\overline{p^*_{Di}}(t_D)$ term in Eq. (117) can be obtained by integrating Eq. (109):

$$\overline{p^*_{Di}}(t_D) = \begin{cases} \text{if } i = 0: \\ \dfrac{1}{\sqrt{N_{\psi_0}}} \displaystyle\sum_{m=1}^{\infty} \overline{\psi}_{0m} \frac{\xi_m(h_{wD}) \widetilde{\Omega}_m(\mathbf{x_{wD}})}{k_{wD}} T_{0m}(t_D) \\ \text{if } i \geq 1: \\ \dfrac{1}{\sqrt{N_{\psi_i}}} \left[-\overline{\psi}_{i0} \xi_0(h_{wD}) \widetilde{\Omega}_0(\mathbf{x_{wD}}) T_{i0}(t_D) + \right. \\ \left. + \displaystyle\sum_{m=1}^{\infty} \overline{\psi}_{im} \frac{\xi_m(h_{wD}) \widetilde{\Omega}_m(\mathbf{x_{wD}})}{k_{wD}} T_{im}(t_D) \right] \end{cases} \tag{121}$$

where $T_{im}(t_D)$ is given by Eq. (110) and where

$$\xi_m(h_{wD}) = \begin{cases} \text{if } m_z = 0: \\ 1 \\ \text{if } m_z \geq 1: \\ \dfrac{2}{h_{wD} \nu_{m_z}} \sin\left(\dfrac{h_{wD}}{2} \nu_{m_z}\right) \end{cases} \tag{122}$$

with index m_z standing for the one-dimensional eigenvalue in the z direction corresponding to the mth three-dimensional eigenvalue in the chosen global reordering. The time derivative is taken directly from Eq. (121):

$$\frac{d\overline{p^*_{Di}}}{dt_D} = \begin{cases} \text{if } i = 0: \\ \dfrac{1}{\sqrt{N_{\psi_0}}} \displaystyle\sum_{m=1}^{\infty} \overline{\psi}_{0m} \frac{\xi_m(h_{wD}) \widetilde{\Omega}_m(\mathbf{x_{wD}})}{k_{wD}} \frac{dT_{0m}}{dt_D} \\ \text{if } i \geq 1: \\ \dfrac{1}{\sqrt{N_{\psi_i}}} \left[-\overline{\psi}_{i0} \xi_m(h_{wD}) \widetilde{\Omega}_0(\mathbf{x_{wD}}) \dfrac{dT_{i0}}{dt_D} + \right. \\ \left. + \displaystyle\sum_{m=1}^{\infty} \overline{\psi}_{im} \frac{\xi_m(h_{wD}) \widetilde{\Omega}_m(\mathbf{x_{wD}})}{k_{wD}} \frac{dT_{im}}{dt_D} \right] \end{cases} \tag{123}$$

with $\frac{dT_{im}}{dt_D}$ given by Eq. (112).

The $F_D(\mathbf{x_D}, t_D)$ and $\frac{\partial F_D}{\partial t_D}$ terms in Eqs. (117) and (120) are obtained by integrating Eqs. (81) and (82):

$$F_D(\mathbf{x_D}, t_D) = \xi_0(h_{wD}) \widetilde{\Omega}_0(\mathbf{x_{wD}}) \widetilde{\Omega}_0(\mathbf{x_D}) t_D + \\ + \sum_{j=1}^{\infty} \frac{\xi_j(h_{wD}) \widetilde{\Omega}_j(\mathbf{x_{wD}}) \widetilde{\Omega}_j(\mathbf{x_D})}{k_{wD} \eta_j^2} \left(1 - e^{-k_{wD} \eta_j^2 t_D}\right), \tag{124}$$

$$\frac{\partial F_D}{\partial t_D} = \sum_{j=0}^{\infty} \xi_j(h_{wD}) \widetilde{\Omega}_j(\mathbf{x_{wD}}) \widetilde{\Omega}_j(\mathbf{x_D}) e^{-k_{wD} \eta_j^2 t_D}. \tag{125}$$

Or, alternatively, by integrating Eqs. (83) and (84):

$$F_D(\mathbf{x_D}, t_D) = \int_0^{t_D} \frac{\partial F_D}{\partial t_D} d\tau, \tag{126}$$

$$\frac{\partial F_D}{\partial t_D} = \sum_{j=0}^{\infty} \frac{(-1)^{l(j)}}{8\pi h_{wD} k_{wD} t_D} \exp\left(-\frac{r_{Dj}^2}{4 k_{wD} t_D}\right) \cdot \\ \cdot \left[\operatorname{erf}\left(\frac{f_{z,l(j)}}{2\sqrt{k_{wD} t_D}}\right) - \operatorname{erf}\left(\frac{f_{z,(l+1)(j)}}{2\sqrt{k_{wD} t_D}}\right) \right], \tag{127}$$

which correspond to Eqs. (B.1) and (B.8) when $k_{wD} = 1$.

It should be noted that the eigenvalues μ_i and the eigenfunctions $\widetilde{\psi}_i(\mathbf{x_D})$ depend only on the domain's heterogeneity, and not on the geometry of the source or sink. Therefore, their expressions are identical to the ones calculated for the point-source in Eqs. (91)–(102), and they would remain the same for any other well geometry.

4.3.1. Approximate infinite conductivity solution

The problem of using uniform *flow* expressions to approximate the solution within the wellbore (which effectively displays uniform *pressure*) is well known, and various methods have been proposed — the most flexible and accurate (Biryukov and Kuchuk, 2012a) of which is averaging the pressure along the wellbore (Streltsova-Adams, 1979):

$$p_{wD}(x_D, y_D, t_D) = \frac{1}{h_{wD}} \int_{z_{wD}-h_{wD}/2}^{z_{wD}+h_{wD}/2} p_D(\mathbf{x_D}, t_D) dz_D \tag{128}$$

Substituting Eq. (117) into Eq. (128) yields

$$p_{wD}(x_D, y_D, t_D) = F_{wD}(x_D, y_D, t_D) + \sum_{i=0}^{\infty} \overline{p^*_{Di}}(t_D) \widetilde{\psi}_{z,i}(x_D, y_D), \tag{129}$$

where

$$\widetilde{\psi}_{z,i}(x_D, y_D) = \frac{1}{\sqrt{N_{\psi_i}}} \sum_{m=0}^{\infty} \overline{\psi}_{im} \widetilde{\Omega}_m(x_D, y_D, z_{wD}) \xi_m(h_{wD}), \tag{130}$$

and $F_{wD}(x_D, y_D, t_D)$ obtained either from Eq. (124):

$$F_{wD}(x_D, y_D, t_D) = \xi_j^2(h_{wD}) \widetilde{\Omega}_0(\mathbf{x_{wD}}) \widetilde{\Omega}_0(x_D, y_D, z_{wD}) t_D + \\ + \sum_{j=1}^{\infty} \frac{\xi_j^2(h_{wD}) \widetilde{\Omega}_j(\mathbf{x_{wD}}) \widetilde{\Omega}_j(x_D, y_D, z_{wD})}{k_{wD} \eta_j^2} \left(1 - e^{-k_{wD} \eta_j^2 t_D}\right), \tag{131}$$

or from Eq. (126):

$$F_{wD}(x_D, y_D, t_D) = \int_0^{t_D} \frac{\partial F_{wD}}{\partial t_D} d\tau. \tag{132}$$

Table 2
Numerical properties for the point-source application examples.

Parameters	Values	Units
Flowrate, q	70	$m^3\,d^{-1}$
Permeability in x, k_x	2000	mD
Permeability in y, k_y	2000	mD
Permeability in z, k_z	20	mD
Porosity, ϕ	30	%
Viscosity, μ_f	1×10^{-3}	Pa s
Compressibility, c_t	2.5493×10^{-6}	kPa^{-1}
Initial pressure, p_i	29 419.95	kPa
Well radius, r_w	0.120 65	m
Reservoir x length, L_x	2400	m
Reservoir y length, L_y	2400	m
Reservoir z length, L_z	30	m
Point-source x coordinate, x_w	1200	m
Point-source y coordinate, y_w	1200	m
Point-source z coordinate, z_w	15	m

The time derivatives for Eqs. (129), (131) and (132) are, respectively,

$$\frac{\partial p_{wD}}{\partial t_D} = \frac{\partial F_{wD}}{\partial t_D} + \sum_{i=0}^{\infty} \frac{d\overline{p^*_{Di}}}{dt_D}\widetilde{\psi}_{z,i}(x_D, y_D), \tag{133}$$

$$\frac{\partial F_{wD}}{\partial t_D} = \sum_{j=0}^{\infty} \xi_j^2(h_{wD})\widetilde{\Omega}_j(\mathbf{x_{wD}})\widetilde{\psi}_{z,i}(x_D, y_D)e^{-k_{wD}\eta_j^2 t_D}, \tag{134}$$

$$\begin{aligned}\frac{\partial F_{wD}}{\partial t_D} = \sum_{i=0}^{\infty} \frac{(-1)^{l(i)}}{8\pi h_{wD}^2 k_{wD} t_D} \exp\left(-\frac{r_{Di}^2}{4k_{wD}t_D}\right)\Big\{ \\ F^+_{z,l(i)}\left(z^+_{wD}, k_{wD}t_D\right) - F^+_{z,l(i)}\left(z^-_{wD}, k_{wD}t_D\right) - \\ -F^-_{z,l(i)}\left(z^+_{wD}, k_{wD}t_D\right) + F^-_{z,l(i)}\left(z^-_{wD}, k_{wD}t_D\right)\Big\},\end{aligned} \tag{135}$$

with $F^+_{z,l(i)}$ and $F^-_{z,l(i)}$ defined in Eqs. (B.11) and (B.12).

It should be noted that only the filter expression $F_D(\mathbf{x_D}, t_D)$ and the auxiliary eigenfunctions $\widetilde{\Omega}_m(\mathbf{x_D})$ required integration to account for the uniform pressure condition at the wellbore. This would remain true for any other well geometry: the transformed filtered potentials $\overline{p^*_{D_i}}(t_D)$ and transformed eigenvectors $\overline{\psi}_{im}$ from the uniform flow solution should always be directly applicable for the corresponding approximate infinite conductivity expression.

5. Results and discussion

5.1. Point-source in a homogeneous reservoir

As pointed out in Section 4.1, the integral transform solution in Eqs. (67) and (68) will not perform adequately for well testing applications. Instead, the equivalent solution obtained by the method of images of Eqs. (A.4) and (A.5) should be preferred for computations during the early transient period. To illustrate this point, the numerical parameters in Table 2 were used to generate the log–log plot of Fig. 2, which compares the drawdown pressure $\Delta p(\mathbf{x}, t)$ and its logarithmic derivative $\partial \Delta p / \partial \ln t$ for each of these alternative expressions at $(x, y, z) = (x_w + r_w, y_w, z_w)$ — the *sandface*. Eqs. (A.4) and (A.5) were evaluated with 900 terms in the summation, whereas Eqs. (67) and (68) are shown with increasing truncation orders.

The derivative in Fig. 2 displays all expected flow regimes: short-term spherical flow near the point-source ($t < 0.5$ h); infinite acting radial flow between the two no-flow boundaries in the z direction ($1.5 < t < 30$ h); and boundary-dominated pseudo-steady state flow ($t > 50$ h). The time interval where the derivative of both solutions match increases with the truncation order of the eigenfunction expansion: convergence happens first at the *late time*, and progressively moves towards the *early time*. Notably, the derivative achieves convergence on the graphical scale at $t > 8$ h with only 10 terms, whereas it requires at least 10 000 terms for $t < 0.03$ h. And even for truncation orders as high as 100 000 terms, the drawdown pressure still differs from the method of images solution by roughly two orders of magnitude.

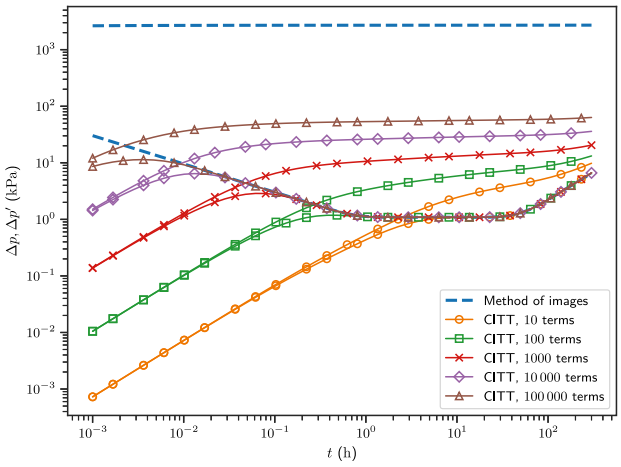

Fig. 2. Log–log plot for the sandface drawdown pressure and its logarithmic derivative calculated by: the classical method of images; and the integral transform (CITT), with increasing truncation orders.

The reason behind the slow convergence behavior of the integral transform in this particular application lies within the structure of the expansion in Eq. (67). The eigenfunctions $\widetilde{\Omega}_i(\mathbf{x_D})$ are purely oscillatory, and thus have no influence on the rate of convergence. Instead, the decay of the infinite summation is produced by the $e^{-\eta_i^2 t_D}/\eta_i^2$ and $1/\eta_i^2$ terms — the second of which is merely inverse square, and thus dominates the rate of convergence. Comparatively, the method of images solution in Eq. (A.4) has exponential decay. The same happens with the time derivative in Eq. (68), which is also driven by exponential decay. Finally, the faster convergence at later times is clearly due to the $e^{-\eta_i^2 t_D}/\eta_i^2$ term — which is also exponentially decreasing with time.

In particular cases where only the derivative is required, this performance could still be reasonable for practical applications. However, the mathematical equivalence between these two solutions demonstrated in Section 4.1.2 allows for the use of the exponential form, with its associated performance advantages, in all subsequent computations.

5.2. Point-source in a heterogeneous reservoir

5.2.1. Layered reservoir

Fig. 3 illustrates a layered reservoir containing three layers of different permeabilities. This is obtained from Eq. (74) by making

$$k_D(\mathbf{x_D}) = \begin{cases} 1, & \frac{1}{3}L_{zD} \le z_D \le \frac{2}{3}L_{zD}, \\ 0.5, & \text{otherwise.} \end{cases} \tag{136}$$

By using Table 2 again for the dimensional parameters, Eq. (136) describes three 10 m layers in the z direction, for a total reservoir thickness of 30 m. The point-source is located at $z_{wD} = 0.5 \cdot L_{zD}$, in the middle of the highest permeability layer, and observation points have been placed in the coordinates relative to the point-source represented in Table 3. These points are logarithmically spaced and progressively farther from the point-source in the x–y plane in order to demonstrate the solution's lateral behavior, and they sample both the higher permeability middle layer and the lower permeability top layer.

Fig. 4 displays the behavior for the drawdown pressure $\Delta p(\mathbf{x}, t)$ and its logarithmic derivative $\partial \Delta p / \partial \ln t$ at $(x, y, z) = (x_w + r_w, y_w, z_w)$ — the *sandface* — using a standard pressure derivative log–log plot and the following solutions:

1. The classical method of images solution for the point-source given by Eqs. (A.4) and (A.5) with 1900 terms in the summation, when the permeability of the middle layer is used for the whole domain.

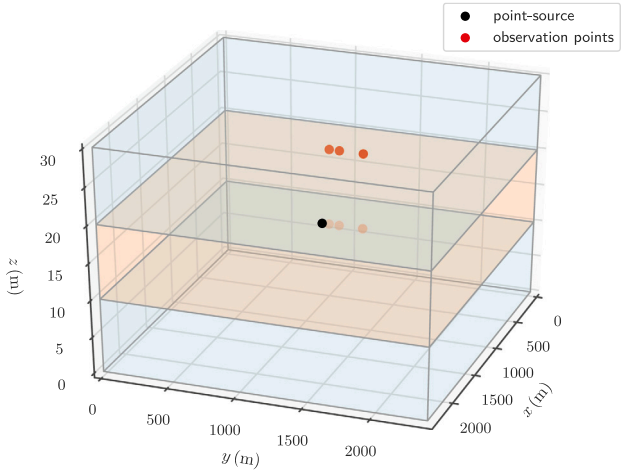

(a) 3D schematic view of the reservoir model.

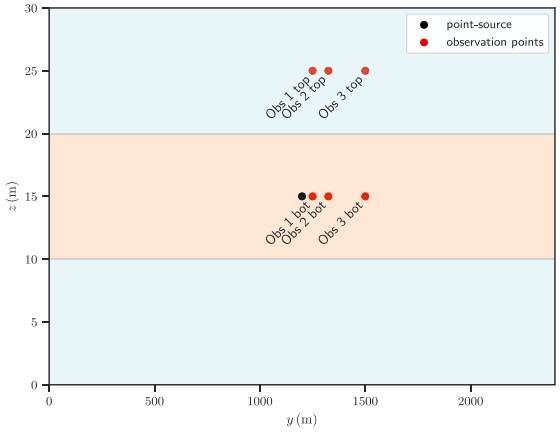

(b) Slice through the $y-z$ plane at $x = x_{wD}$.

Fig. 3. Schematic of the heterogeneous layered reservoir model used with the point-source solution.

Table 3
Layered reservoir observation points' positions relative to the point-source: $\Delta\mathbf{x} = \mathbf{x}_{obs} - \mathbf{x}_{w}$.

Point	Δx(m)	Δy(m)	Δz(m)
Obs 1 bot	0	50	0
Obs 2 bot	0	125	0
Obs 3 bot	0	300	0
Obs 1 top	0	50	10
Obs 2 top	0	125	10
Obs 3 top	0	300	10

2. The same method of images solution using the long-term equivalent horizontal permeability $k_{D\text{equiv}}$ for the heterogeneous three layers model, with 500 terms in the summation:

$$k_D(\mathbf{x_D}) = k_{D\text{equiv}} = \frac{\sum_{i=1}^{3} k_{Di} L_{zDi}}{\sum_{i=1}^{3} L_{zDi}} = \frac{2}{3}. \tag{137}$$

3. A numerical solution for the three layers heterogeneous problem obtained in the commercial reservoir 3D flow simulator *Rubis* (KAPPA, 2017), using an unstructured Voronoi grid with automatic refinement around wells tuned to reproduce short-term pressure transient behavior.

The derivative in Fig. 4 displays all expected flow regimes: short-term spherical flow within the middle layer ($t < 0.1$ h); a transition

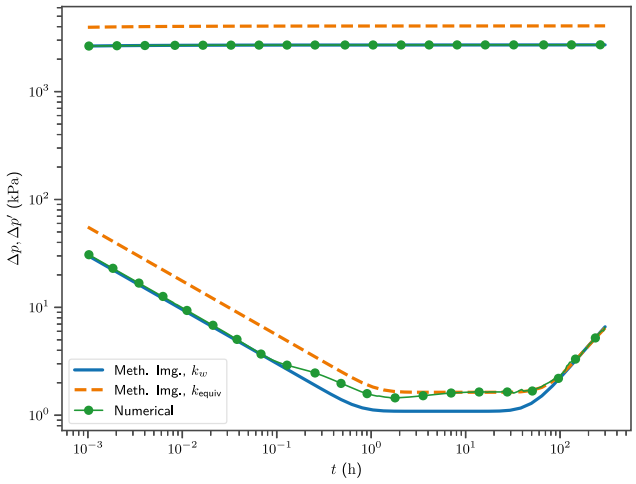

Fig. 4. Log–log plot for the sandface drawdown pressure and its derivative with the analytical method of images and numerical *Rubis* (KAPPA, 2017) solutions of the layered reservoir problem.

Table 4
Convergence behavior in a sample of the first 30 eigenvalues for the layered reservoir problem, with increasing truncation orders.

μ_i	$n(m)$, where $m = n + \Delta n$					
	100 (110)	500 (580)	1000 (1350)	2000 (2781)	8000 (11 338)	12 000 (17 086)
1	0.0000	0.0000	0.0000	0.0000	0.0000	0.0000
2	1.2825	1.2823	1.2823	1.2823	1.2823	1.2823
3	1.2825	1.2823	1.2823	1.2823	1.2823	1.2823
4	1.8138	1.8131	1.8131	1.8131	1.8131	1.8131
5	2.5651	2.5632	2.5632	2.5632	2.5631	2.5631
6	2.5651	2.5632	2.5632	2.5632	2.5631	2.5631
7	2.8679	2.8652	2.8652	2.8652	2.8651	2.8651
8	2.8679	2.8652	2.8652	2.8652	2.8651	2.8651
9	3.6276	3.6222	3.6222	3.6222	3.6220	3.6220
10	3.8476	3.8412	3.8412	3.8412	3.8410	3.8410
15	4.6243	4.6132	4.6132	4.6132	4.6128	4.6128
20	5.4414	5.4233	5.4233	5.4233	5.4227	5.4227
25	6.4127	6.3832	6.3832	6.3832	6.3823	6.3823
30	6.9067	6.8699	6.8699	6.8699	6.8688	6.8688

influenced by the top and bottom layers, as well as the no-flow boundaries in the z direction ($0.1 < t < 5$ h); infinite acting radial flow with $k_D(\mathbf{x_D}) = k_{D\text{equiv}}$ as in Eq. (137) ($5 < t < 50$ h); and boundary-dominated pseudo-steady state flow ($t > 50$ h). The analytical homogeneous reservoir solutions are shown as limiting cases: the $k_D(\mathbf{x_D}) = 1$ solution is in agreement with the numerical model in the short-term, whereas the $k_D(\mathbf{x_D}) = k_{D\text{equiv}}$ solution matches the system's long-term behavior, with the heterogeneous numerical model transitioning between these two limits in the middle-time region.

Table 4 displays the convergence in a sample of the first 30 eigenvalues of the GITT solution, with a truncation order of $m = n + \Delta n$ terms in the eigenvalue problem: n auxiliary eigenvalues η_i selected in order of increasing magnitude; and Δn additional terms from the main diagonal of the $\mathbf{B}^{-1}\mathbf{A}$ matrix. In order to understand the small differences appearing between the decimal digits as the truncation order increases, it is important to consider Table 5 with the number of distinct one-dimensional eigenvalues selected in each orthogonal direction. In reservoir applications, the domain is usually much smaller in the z direction than in the x and y directions. For the current example, the domain's dimensionless lengths obey the following relationships: $L_{xD}/L_{yD} = 1$ and $L_{xD}/L_{zD} = L_{yD}/L_{zD} = 8$. Consequently, according to Eq. (64), the auxiliary one-dimensional eigenvalues in the x and y directions will have much lower magnitudes than those in the z direction, meaning they will be sorted first by the criterion of increasing

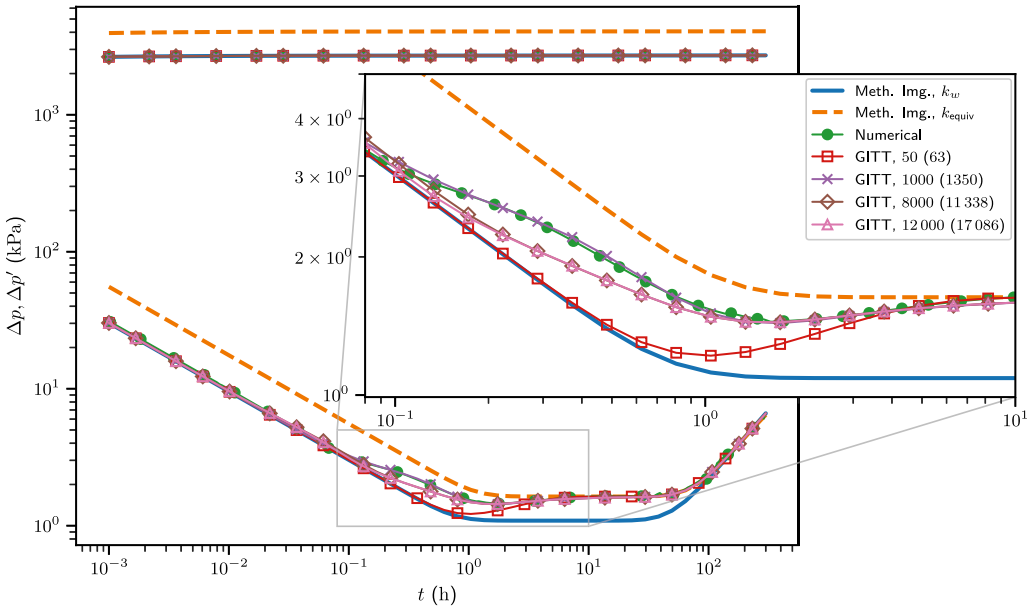

Fig. 5. Layered reservoir numerical *Rubis* (KAPPA, 2017) and GITT solutions at the point-source, with increasing truncation orders.

Table 5
Number of distinct one-dimensional eigenvalues selected in each orthogonal direction for the layered reservoir problem, with increasing truncation orders.

n (m)	1D eigenvalues		
	x	y	z
50 (63)	8	8	2
100 (110)	10	10	2
500 (580)	20	20	3
1000 (1350	26	26	4
2000 (2781)	34	34	5
8000 (11 338)	56	56	8
12 000 (17 086)	65	65	8

magnitude. A comparison of Tables 4 and 5 suggests a correlation between the inclusion of additional terms in the z direction and the differences appearing in the first few digits of the eigenvalues. Although the additional reordering criterium complements the selection of terms, increasing the participation of the z direction, further improvement can be envisioned through a new more comprehensive criterium or a second reordering pass.

Fig. 5 and Table 6 show a comparison between the GITT results at the sandface, with increasing truncation orders, and the other methods' solutions previously shown in Fig. 4. The eigenvalue problem is always truncated to the same order as the potential, in each case. The filter expression, which is the homogeneous reservoir solution in its exponential form (Eqs. (A.4) and (A.5)), was calculated with 1900 terms in the summation. While the solutions are in good agreement, the convergence rate is not uniform: 50 terms in the eigenfunction expansion are enough for all but the 0.1 to 6 hours interval; 1000 terms reduce this to between 0.1 and 1 hours; and 8000 terms further restrict this to a small interval around 0.1 hour, which still oscillates even after 12 000 terms. Since Table 4 shows the eigenvalue problem to be practically converged after only 100 terms, the 8000 terms requirement for the potential must be caused by the filtered source term itself, which starts deviating from the solution once the top and bottom layers start to have an effect on the pressure response measured at the point-source.

Figs. 6(a) and 6(b) display the GITT solution's pressure derivative behavior at the chosen observation points, truncated to 1000 and 12 000 terms. It is mostly in good agreement with the numerical solution, except for points *Obs 1 bot* and *Obs 1 top* which are the closest to the

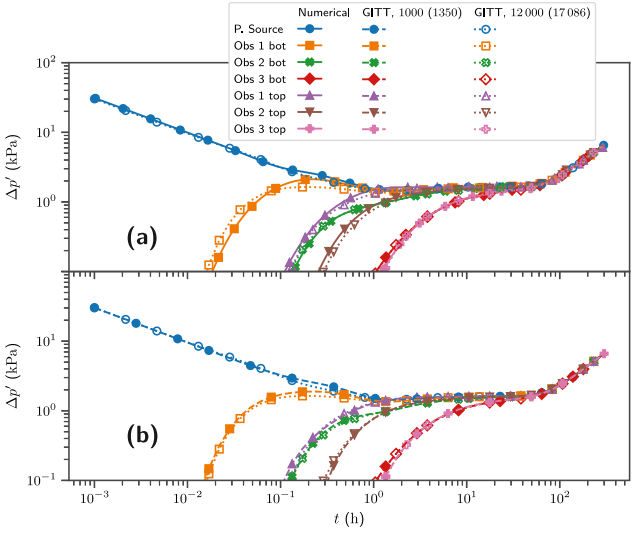

Fig. 6. Layered reservoir. (a) Numerical *Rubis* (KAPPA, 2017) and GITT solution at the observation points, truncated to 1000 (1350) terms. (b) Comparison of GITT solutions with 1000 (1350) and 12 000 (17 086) terms.

point-source in the x–y plane. The non-uniform rate of convergence is also apparent when comparing both truncation orders, as the only observation point with any significant difference is *Obs 1 bot* — which is closest to the point-source.

5.2.2. Linear channel reservoir

Fig. 7 illustrates a reservoir containing a higher permeability linear channel. This is obtained from Eq. (74) by making

$$k_D(\mathbf{x_D}) = \begin{cases} 1, & \frac{5}{12}L_{xD} \le x_D \le \frac{7}{12}L_{xD}, \\ 0.5, & \text{otherwise.} \end{cases} \tag{138}$$

By using Table 2 again for the dimensional parameters, Eq. (138) describes a 400 m wide region in a total reservoir x length of 2400 m. The point-source is located at $x_{wD} = 0.5 \cdot L_{xD}$, in the middle of the higher permeability region, and observation points have been placed in the coordinates relative to the point-source represented in Table 7.

Table 6
Convergence behavior for the sandface drawdown pressure and its logarithmic derivative for the layered reservoir problem, with increasing truncation orders.

Time (h)	50 (63)	100 (110)	500 (580)	2000 (2781)	8000 (11 338)	12 000 (17 086)	Rubis
	$\Delta p(\mathbf{x}_w, t) = p_i - p(\mathbf{x}_w, t)$ (kPa)						
0.01	2688.2	2688.2	2688.2	2688.2	2688.2	2688.2	2688.2
0.1	2701.2	2701.2	2701.3	2701.5	2701.7	2701.7	2701.6
1	2705.5	2705.5	2706.3	2706.8	2706.6	2706.5	2706.9
10	2708.8	2709.0	2709.9	2710.3	2710.0	2710.0	2710.4
100	2712.8	2713.0	2713.8	2714.2	2714.0	2713.9	2714.4
	$\Delta p'(\mathbf{x}_w, t) = \partial \Delta p / \partial \ln t$ (kPa)						
0.01	9.5587	9.5588	9.5598	9.5689	9.6089	9.6323	9.9203
0.1	3.0243	3.0261	3.0986	3.3910	3.2334	3.1229	3.1321
1	1.2183	1.2963	1.6775	1.4853	1.4902	1.4902	1.5479
10	1.6301	1.6331	1.5892	1.5890	1.5902	1.5902	1.6332
100	2.3354	2.3354	2.3343	2.3343	2.3344	2.3344	2.2745

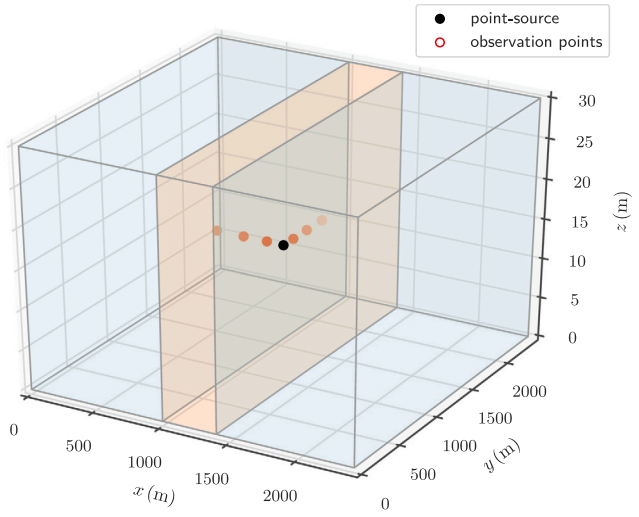

(a) 3D schematic view of the reservoir model.

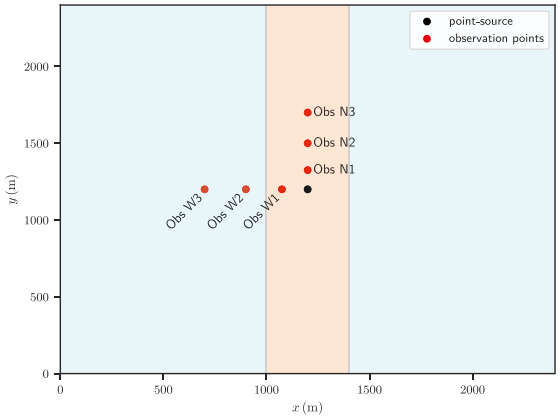

(b) Slice through the $x - y$ plane at $z = z_{wD}$.

Fig. 7. Schematic of the heterogeneous channel reservoir model used with the point-source solution.

These points are logarithmically spaced and progressively farther from the point-source both within the channel and crossing into the lower permeability outer region; the sampling is restricted to the x–y plane, as the system is effectively homogeneous along z.

Fig. 8 displays the behavior for the drawdown pressure $\Delta p(\mathbf{x}, t)$ and its logarithmic derivative $\partial \Delta p / \partial \ln t$ at $(x, y, z) = (x_w + r_w, y_w, z_w)$ — the *sandface* — using a standard pressure derivative log–log plot and the following solutions:

Table 7
Linear channel reservoir observation points' positions relative to the point-source: $\Delta \mathbf{x} = \mathbf{x}_{obs} - \mathbf{x}_w$.

Point	Δx(m)	Δy(m)	Δz(m)
Obs N1	0	125	0
Obs N2	0	300	0
Obs N3	0	500	0
Obs W1	−125	0	0
Obs W2	−300	0	0
Obs W3	−500	0	0

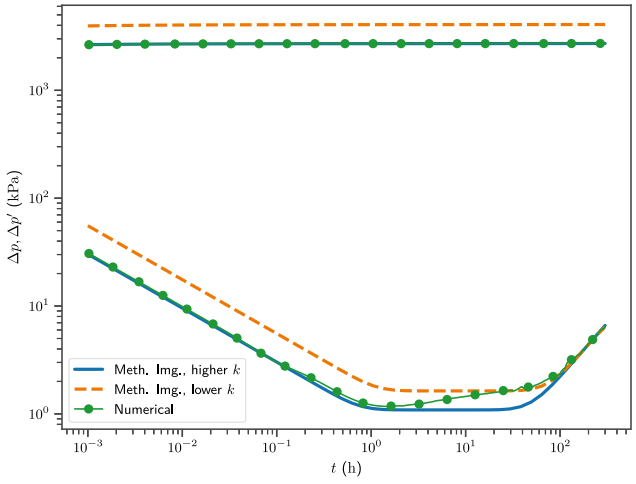

Fig. 8. Log–log plot for the sandface drawdown pressure and its derivative with the analytical method of images and numerical *Rubis* (KAPPA, 2017) solutions of the linear channel reservoir problem.

1. The classical method of images solution for the point-source given by Eqs. (A.4) and (A.5) with 1900 terms in the summation, when the higher permeability within the channel is used for the whole domain.
2. The same method of images solution using the lower permeability outside the channel for the whole domain, with 500 terms in the summation.
3. A numerical solution for the linear channel heterogeneous problem obtained in the commercial reservoir 3D flow simulator *Rubis*, using an unstructured Voronoi grid with automatic refinement around wells tuned to reproduce short-term pressure transient behavior.

Table 8
Convergence behavior in a sample of the first 30 eigenvalues for the linear channel reservoir problem, with increasing truncation orders.

μ_i	$n(m)$, where $m = n + \Delta n$					
	50 (56)	100 (115)	200 (247)	500 (613)	1000 (1188)	10 000 (12 765)
1	0.0000	0.0000	0.0000	0.0000	0.0000	0.0000
2	1.1928	1.1928	1.1927	1.1927	1.1927	1.1926
3	1.2200	1.2189	1.2182	1.2157	1.2149	1.2125
4	1.6508	1.6500	1.6495	1.6476	1.6470	1.6453
5	2.2456	2.2405	2.2396	2.2393	2.2384	2.2377
6	2.3520	2.3520	2.3516	2.3514	2.3513	2.3512
7	2.5368	2.5362	2.5359	2.5347	2.5343	2.5331
8	2.5751	2.5722	2.5703	2.5701	2.5695	2.5690
9	3.3805	3.3784	3.3779	3.3777	3.3775	3.3774
10	3.4743	3.4742	3.4734	3.4732	3.4730	3.4727
15	4.3944	4.3932	4.3929	4.3922	4.3922	4.3919
20	4.9616	4.9557	4.9555	4.9499	4.9480	4.9435
25	5.8090	5.7821	5.7755	5.7706	5.7688	5.7648
30	6.5287	6.5174	6.5127	6.5103	6.5097	6.5078

Table 9
Number of distinct one-dimensional eigenvalues selected in each orthogonal direction for the linear channel reservoir problem, with increasing truncation orders.

n (m)	1D eigenvalues		
	x	y	z
50 (56)	8	9	2
100 (115)	11	11	2
200 (247)	14	15	2
500 (613)	19	21	3
1000 (1188)	25	27	4
10 000 (12 765)	56	61	8

The derivative in Fig. 8 displays all expected flow regimes: short-term spherical flow ($t < 1$ h); a transition in which the higher permeability channel receives pressure support from outside ($1 < t < 50$ h), skipping infinite acting radial flow entirely due to the channel's reduced width; and boundary-dominated pseudo-steady state flow ($t > 50$ h). The analytical homogeneous reservoir solutions are shown as limiting cases: the $k_D(\mathbf{x_D}) = 1$ solution is in agreement with the numerical model in the short-term, whereas the $k_D = 0.5$ solution matches the system's long-term behavior, with the heterogeneous numerical model transitioning between these two limits in the middle-time region.

Table 8 displays the convergence in a sample of the first 30 eigenvalues of the GITT solution, with a truncation order of $m = n + \Delta n$ terms in the eigenvalue problem: n auxiliary eigenvalues η_i selected in order of increasing magnitude; and Δn additional terms from the main diagonal of the $\mathbf{B}^{-1}\mathbf{A}$ matrix. Small differences appear between the first decimal digits as the truncation order increases, much like what happened in the layered reservoir problem. Tables 5 and 9 show a comparable number of distinct one-dimensional eigenvalues, even though the heterogeneity in each problem has very distinct characteristics. The similarity lies in the domain's lengths in each direction, which dictate the reordering criterion of increasing magnitude. Therefore, it is clear that this criterion is dominant over the heterogeneity one in terms of selecting elements for the $\mathbf{A}$ matrix of the algebraic eigenvalue problem.

Fig. 9 and Table 10 show a comparison between the GITT results at the sandface, with increasing truncation orders, and the other methods' solutions, already shown in Fig. 8. The eigenvalue problem is always truncated to the same order as the potential, in each case. The filter expression, which is the homogeneous reservoir solution in its exponential form (Eqs. (A.4) and (A.5)), was calculated with 1900 terms in the summation. The pressure derivative is practically converged on the graphical scale with only 200 terms, unlike the 8000 terms which were required for the layered reservoir. In order to understand this significant performance difference, it should be noted that:

1. The layered reservoir exhibits essentially homogeneous behavior until 0.1 hour, when the top and bottom layers start to have an effect on the pressure response. For the channel reservoir, the homogeneous behavior lasts 1 hour before the channel boundary is perceived.
2. It was previously demonstrated that the classical method of images and the CITT produce alternative forms of the same solution, with distinct convergence characteristics: the first converges rapidly in early times, whereas the second performs better at late time.
3. The chosen filter for this problem is the method of images solution for a homogeneous reservoir.

An alternative interpretation for Eq. (21) is that the GITT solution for the filtered problem is simply a correction term to be applied to the homogeneous solution in order to take into account the reservoir's heterogeneity. Since the filter expression converges rapidly in early times and the GITT performs better at late time, the earlier the GITT correction term has to be applied to the homogeneous solution, the larger the number of terms required to reach convergence.

Figs. 10(a) and 10(b) displays the GITT solution's pressure derivative behavior at the chosen observation points, truncated to 200 and 2000 terms. It is mostly in good agreement with the numerical solution, and no significant difference can be seen between these two truncation orders, except for points *N1* and *W1* — which are closest to the point-source. While the pressure interferences at these closest points are practically indistinguishable in either direction, the higher permeability within the channel causes it to be perceived earlier at *N3* than at *W3*, as expected.

5.2.3. Compartmentalized reservoir

Fig. 11 illustrates a reservoir containing: two disjoint compartments V_1 and V_2 with the same permeabilities; a region V_3 of very low permeability which separates V_1 from V_2; a high permeability layer V_4 cutting through both compartments at the reservoir's bottom boundary; and a very high permeability region V_5 next to the outer boundary of V_2. This is obtained from Eq. (113) by making

$$k_D(\mathbf{x_D}) = \begin{cases} 1, & \text{in } V_1 \text{ and } V_2 \\ 1\times10^{-4}, & \text{in } V_3 \\ 10, & \text{in } V_4 \\ 100, & \text{in } V_5 \end{cases} \tag{139}$$

where

$$\begin{aligned} V_1 &: 0 < x_D < \frac{3}{5}L_{xD},\ 0 < y_D < L_{yD},\ \frac{1}{11}L_{zD} < z_D < L_{zD}, \\ V_2 &: \frac{18}{25}L_{xD} < x_D < L_{xD},\ 0 < y_D < \frac{4}{5}L_{yD},\ \frac{1}{11}L_{zD} < z_D < L_{zD}, \\ V_3 &: \frac{3}{5}L_{xD} < x_D < \frac{18}{25}L_{xD},\ 0 < y_D < L_{yD},\ \frac{1}{11}L_{zD} < z_D < L_{zD}, \\ V_4 &: \left\{0 < x_D < \frac{18}{25}L_{xD},\ 0 < y_D < 1,\ 0 < z_D < 1\right\} \cup \\ &\quad \cup \left\{\frac{18}{25}L_{xD} < x_D < L_{xD},\ 0 < y_D < \frac{4}{5}L_{yD}, 0 < z_D < \frac{1}{11}L_{zD}\right\} \\ V_5 &: \frac{18}{25}L_{xD} < x_D < L_{xD},\ \frac{4}{5}L_{yD} < y_D < L_{yD},\ 0 < z_D < L_{zD}. \end{aligned} \tag{140}$$

Using numerical values from Table 11 for the dimensional parameters, a limited entry vertical well is placed in region V_1, and observation points are chosen in the coordinates relative to the center of the well represented in Table 12, in order to demonstrate the influence of the higher permeability regions in the propagation of the pressure interference.

Fig. 12 displays the behavior for the drawdown pressure $\Delta p_w(\mathbf{x}, t)$ and its logarithmic derivative $\partial \Delta p_w / \partial \ln t$ at $(x, y) = (x_w + r_w, y_w)$ — the approximate infinite conductivity solution at the sandface — using a standard pressure derivative log–log plot and the following solutions:

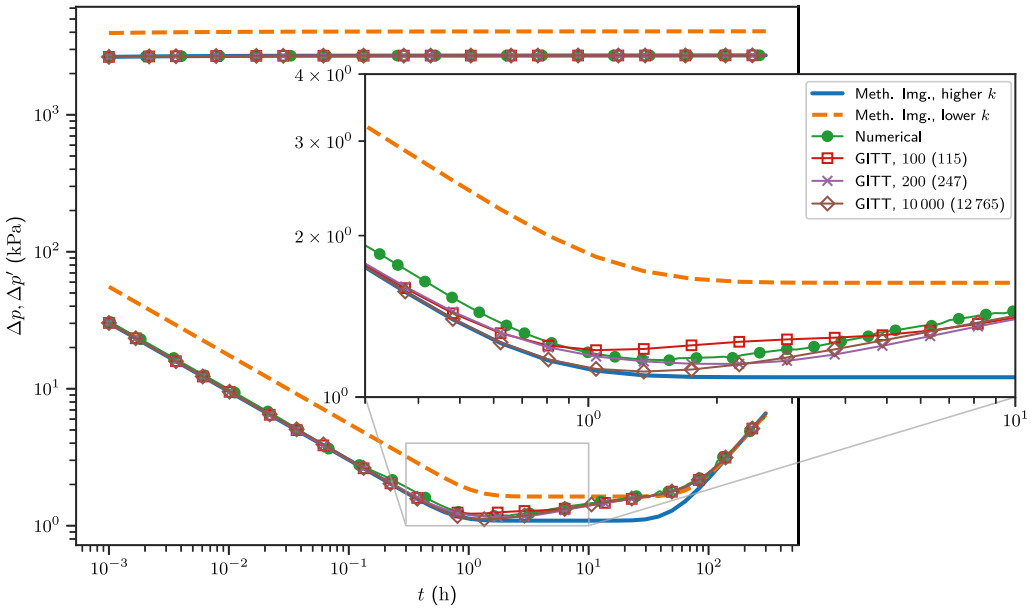

Fig. 9. Linear channel reservoir numerical *Rubis* (KAPPA, 2017) and GITT solutions at the point-source, with increasing truncation orders.

Table 10
Convergence behavior for the sandface drawdown pressure and its logarithmic derivative for the linear channel reservoir problem, with increasing truncation orders.

Time (h)	50 (56)	100 (115)	200 (247)	500 (613)	1000 (1188)	5000 (6434)	10 000 (12 765)	Rubis
	$\Delta p(\mathbf{x}_w, t) = p_i - p(\mathbf{x}_w, t)$ (kPa)							
0.01	2688.2	2688.2	2688.2	2688.2	2688.2	2688.2	2688.2	2688.2
0.1	2701.2	2701.2	2701.2	2701.3	2701.3	2701.3	2701.4	2701.6
1	2705.5	2705.5	2705.5	2705.6	2705.6	2705.6	2705.6	2706.1
2	2706.3	2706.4	2706.3	2706.3	2706.3	2706.3	2706.4	2706.9
10	2708.6	2708.5	2708.3	2708.3	2708.4	2708.4	2708.4	2709.0
100	2712.5	2712.4	2712.3	2712.3	2712.3	2712.3	2712.3	2713.0
	$\Delta p'(\mathbf{x}_w, t) = \partial \Delta p / \partial \ln t$ (kPa)							
0.01	9.5587	9.5587	9.5588	9.5591	9.5596	9.5655	9.5747	9.9124
0.1	3.0242	3.0253	3.0275	3.0464	3.0628	3.0840	3.0580	3.0160
1	1.2045	1.2246	1.1962	1.1381	1.1253	1.1259	1.1336	1.2114
2	1.2720	1.2595	1.1517	1.1057	1.1328	1.1310	1.1372	1.1877
10	1.4576	1.4061	1.3979	1.4045	1.4160	1.4153	1.4177	1.4486
100	2.4269	2.4263	2.4267	2.4272	2.4288	2.4288	2.4291	2.3609

1. The classical method of images solution for the limited entry vertical well given by Eqs. (B.9) and (B.10) with 539 terms in the summation (7, 7 and 11 terms in directions x, y and z, respectively), when the permeability in region V_1 is used for the whole domain.
2. Two numerical solutions obtained in the commercial reservoir 3D flow simulator *Rubis*, using an unstructured Voronoi grid with automatic refinement around wells tuned to reproduce short-term pressure transient behavior: one for a homogeneous reservoir with the permeability in V_1; the other for the heterogeneous reservoir described by the 5 regions in Eq. (139).

The derivative in Fig. 12 displays the following flow regimes: early-time radial flow within the perforated interval ($t < 0.01$ h); spherical flow due to the vertical investigation of the reservoir ($0.01 < t < 1$ h); a transition which resembles radial flow when the top and bottom no-flow boundaries have been reached ($2 < t < 6$ h); classic *U-Shaped* reservoir flow due to the north, south and west no-flow boundaries ($10 < t < 80$ h); and boundary-dominated pseudo-steady state flow ($t > 80$ h). As all solutions were calculated with the same reservoir thickness L_z, the higher equivalent transmissibility of the heterogeneous model within the transition period ($2 < t < 6$ h) is caused by the higher permeability of layer V_4.

Table 13 displays the convergence in a sample of the first 30 eigenvalues of the GITT solution, with a truncation order of $m = n + \Delta n$ terms in the eigenvalue problem: n auxiliary eigenvalues η_i selected in order of increasing magnitude; and Δn additional terms from the main diagonal of the $\mathbf{B}^{-1}\mathbf{A}$ matrix. It is clear from comparing Tables 4, 8 and 13 that the required truncation order for this eigenvalue problem is much higher than those in previous sections. Likewise, a comparison of Tables 5, 9 and 14 shows that the number of distinct one-dimensional eigenvalues selected in each orthogonal direction by the heterogeneity criterion is also higher. This result can be explained by comparing Eqs. (136), (138) and (139): while previous examples had the heterogeneity $k_D(\mathbf{x_D})$ restricted to a single direction and taking values in the 0.5 to 1 range, in this case $k_D(\mathbf{x_D})$ varies: from 1 ($V_1 \cup V_2$) to 10 (V_4) in the z direction; from 1 (V_2) to 100 (V_5) in the y direction; and from 1×10^{-4} (V_3) to 100 (V_5) in the z direction. It is reasonable to expect a higher number of terms in the eigenvalue problem for such a heterogeneous domain.

Fig. 13 and Table 15 show a comparison between the GITT results at the sandface, with increasing truncation orders, and the other methods' solutions, already shown in Fig. 12. The eigenvalue problem is always truncated to the same order as the potential, in each case. The filter expression, which is the homogeneous reservoir solution (Eqs. (B.9) and (B.10)), was calculated with 539 terms in the summation (7, 7 and 11

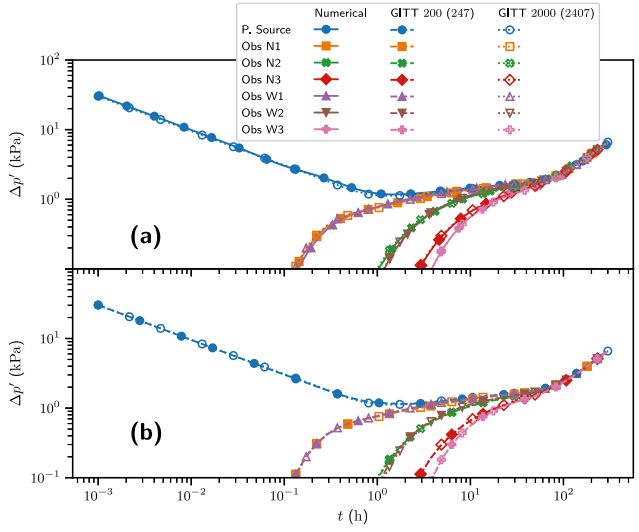

Fig. 10. Linear channel reservoir. (a) Numerical *Rubis* (KAPPA, 2017) and GITT solution at the observation points, truncated to 200 (247) terms. (b) Comparison of GITT solutions with 200 (247) and 2000 (2407) terms.

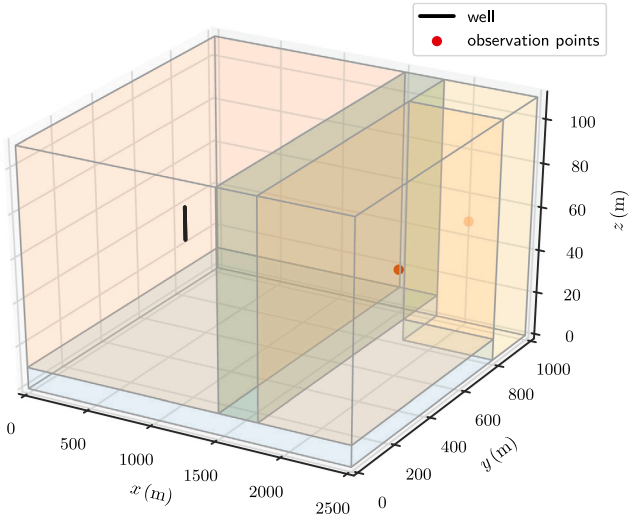

(a) 3D schematic view of the reservoir model.

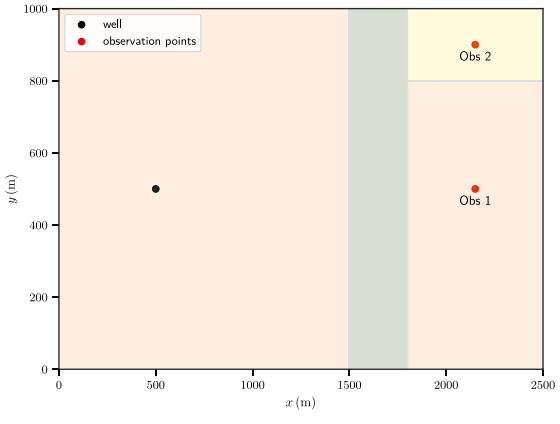

(b) Slice through the $x-y$ plane at $z = z_{wD}$.

Fig. 11. Schematic of the compartmentalized reservoir model used with the limited entry vertical well solution.

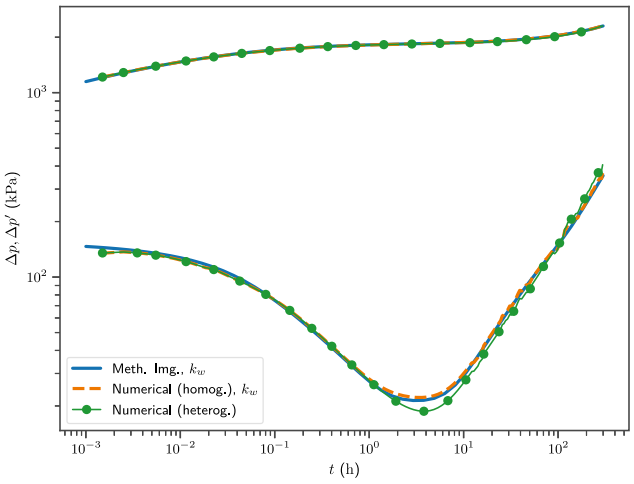

Fig. 12. Log–log plot for the sandface drawdown pressure and its derivative with the analytical method of images and numerical *Rubis* (KAPPA, 2017) solutions of the compartmentalized reservoir problem.

Table 11
Numerical properties for the Limited entry vertical well application example.

Parameters	Values	Units
Flowrate, q	2500	$m^3\ d^{-1}$
Permeability in x, k_x	1000	mD
Permeability in y, k_y	1000	mD
Permeability in z, k_z	50	mD
Porosity, ϕ	15	%
Viscosity, μ_f	1×10^{-3}	Pa s
Compressibility, c_t	2.0394×10^{-6}	kPa^{-1}
Initial pressure, p_i	29 419.95	kPa
Well radius, r_w	0.120 65	m
Reservoir x length, L_x	2500	m
Reservoir y length, L_y	1000	m
Reservoir z length, L_z	110	m
Point-source x coordinate, x_w	500	m
Point-source y coordinate, y_w	500	m
Point-source z coordinate, z_w	55	m
Perforated length, h_w	15	m

Table 12
Compartmentalized reservoir observation points' positions relative to the center of the well: $\Delta\mathbf{x} = \mathbf{x}_{obs} - \mathbf{x}_w$.

Point	Δx(m)	Δy(m)	Δz(m)
Obs 1	1650	0	0
Obs 2	1650	400	0

terms in directions x, y and z, respectively). The pressure derivative is practically converged on the graphical scale with 300 terms, which is similar to the 200 terms required for the linear channel and unlike the 8000 terms for the layered reservoir. It should be noted that the early homogeneous reservoir behavior is much longer in this and the linear channel examples (1 hour) than in the layered reservoir (0.1 hour). This corroborates the already presented discussion: the earlier the GITT correction term has to be applied, the larger the number of terms required to reach convergence.

Figs. 14(a) and 14(b) displays the GITT solution's pressure derivative behavior at the chosen observation points, truncated to 300 and 2000 terms. It is mostly in good agreement with the numerical *Rubis* (KAPPA, 2017) solution, and no significant difference can be seen between these two truncation orders. Even though point *Obs 1* is closer to the well than *Obs 2*, the pressure interference is perceived first at *Obs 2* — which is expected, since *Obs 2* is located within the very high permeability region V_5.

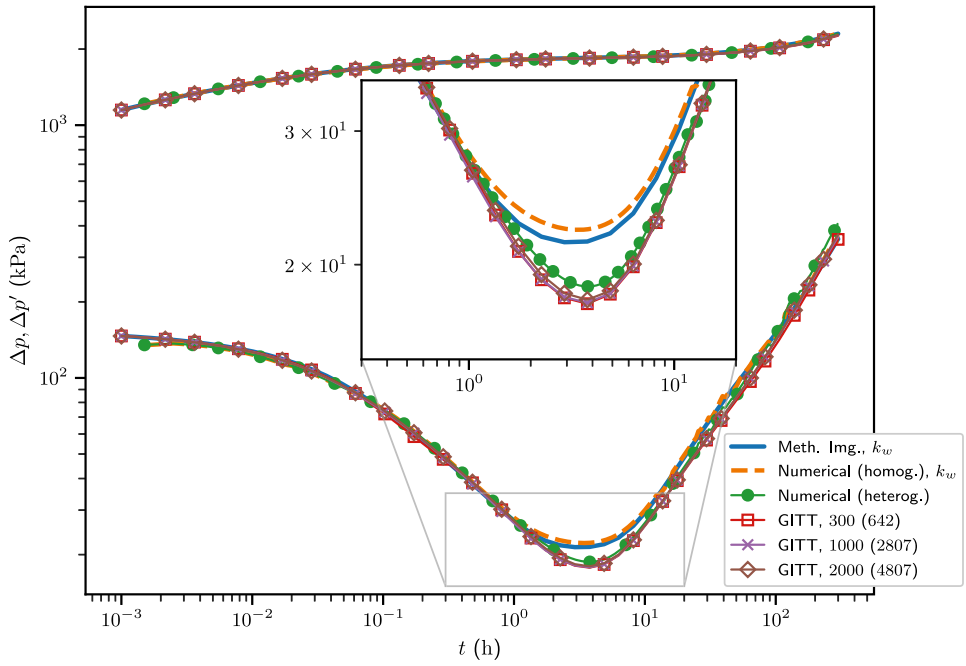

Fig. 13. Compartmentalized reservoir numerical *Rubis* (KAPPA, 2017) and GITT solutions at the well, with increasing truncation orders.

Table 13
Convergence behavior in a sample of the first 30 eigenvalues for the compartmentalized reservoir problem, with increasing truncation orders.

μ_i	$n(m)$, where $m = n + \Delta n$					
	100 (223)	300 (642)	500 (1463)	1000 (2807)	2000 (4807)	3000 (7661)
1	0.0000	0.0000	0.0000	0.0000	0.0000	0.0000
2	1.6432	1.5789	1.4706	0.5648	0.2464	0.1791
3	3.1760	2.9882	1.6980	0.6408	0.2853	0.2078
4	3.8708	3.4224	1.8278	0.8510	0.3579	0.2145
5	4.3943	3.6180	2.0570	0.9262	0.4085	0.2209
6	4.7080	3.8581	2.1050	0.9388	0.4185	0.2391
7	4.9786	4.0592	2.1253	0.9581	0.4347	0.2437
8	5.2810	4.1187	2.1551	0.9635	0.4389	0.2543
9	5.4802	4.1999	2.1831	0.9817	0.4530	0.2558
10	6.1536	4.3083	2.1998	0.9829	0.4556	0.2727
15	7.4885	5.5390	2.7250	1.0429	0.4876	0.3011
20	8.3070	6.9399	3.3110	1.1519	0.5334	0.3326
25	9.1402	7.5202	4.3890	1.4710	0.5642	0.3693
30	9.9298	8.3935	5.1840	1.6505	0.6191	0.3952

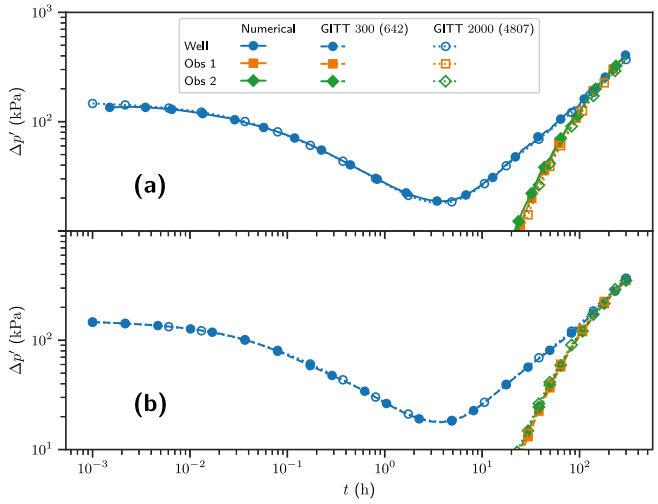

Fig. 14. Compartmentalized reservoir. (a) Numerical *Rubis* (KAPPA, 2017) and GITT solution at the observation points, truncated to 300 (642) terms. (b) Comparison of GITT solutions with 300 (642) and 2000 (4807) terms.

Table 14
Number of distinct one-dimensional eigenvalues selected in each orthogonal direction for the compartmentalized reservoir problem, with increasing truncation orders.

n (m)	1D eigenvalues		
	x	y	z
100 (223)	17	8	4
300 (642)	24	11	6
500 (1463)	33	14	8
1000 (2807)	41	18	10
2000 (4807)	49	22	12
3000 (7661)	58	25	14

Conclusions

The present work provides a novel solution to the continuous point-source problem in heterogeneous reservoirs through the use of the hybrid analytical–numerical approach of the Generalized Integral Transform Technique — GITT. The research suggests this model is the most general and least restrictive expression presented so far to this single problem, capable of handling different permeability regions arbitrarily and irregularly distributed throughout the 3D domain. Although the point-source is an idealized geometry, it was demonstrated in Section 4.3 — using the limited entry vertical well as an example — that this expression can easily be used as a building block to obtain uniform flow solutions in heterogeneous reservoirs for any other well geometry through spatial superposition. The proposed expressions are verified against known analytical models and results from a commercial numerical simulator, and are shown to be in good agreement.

Due to the combined requirements of large domains, short times of interest and spatially concentrated source functions, which are intrinsic to the context of well-test interpretation problems, the computational

Table 15
Convergence behavior for the sandface drawdown pressure and its logarithmic derivative for the compartmentalized reservoir problem, with increasing truncation orders.

Time (h)	100 (223)	200 (334)	300 (642)	400 (709)	500 (1463)	1000 (2807)	2000 (4807)	Rubis
	$\Delta p_w(\mathbf{x_w}, t) = p_i - p_w(\mathbf{x_w}, t)$ (kPa)							
0.01	1468.6	1468.5	1468.5	1468.5	1468.4	1468.2	1468.0	1565.1
0.1	1707.1	1706.7	1706.0	1706.0	1705.0	1704.6	1704.8	1797.9
0.4	1782.6	1782.5	1783.5	1783.8	1783.8	1783.8	1784.5	1878.4
10	1857.6	1858.8	1862.2	1863.4	1862.9	1862.1	1863.9	1959.2
100	2007.6	2009.8	2013.8	2015.0	2016.4	2016.9	2019.2	2121.7
200	2133.9	2136.5	2140.9	2142.3	2144.7	2149.0	2152.5	2265.8
	$\Delta p'_w(\mathbf{x_w}, t) = \partial \Delta p_w / \partial \ln t$ (kPa)							
0.01	127.30	127.27	127.20	127.20	127.02	126.75	126.51	123.64
0.1	73.350	73.023	72.805	72.815	73.050	73.983	74.703	75.207
0.4	38.103	39.178	41.657	42.179	42.313	41.561	42.097	42.237
10	25.818	25.877	25.910	25.926	26.011	25.971	26.067	26.684
100	133.11	133.97	134.72	134.87	136.81	140.06	140.71	143.03
200	245.33	245.58	245.87	245.93	246.84	254.38	257.97	279.66

performance of the inverse formula was found to be slower when the early homogeneous reservoir behavior was very short. Future works may explore additional convergence acceleration techniques to reduce the required truncation orders in the algebraic eigenvalue problem and the eigenfunction expansion, such as three-dimensional integral balance procedures (Cotta et al., 2016) and virtual moving boundaries (Naveira et al., 2009). Furthermore, as this formulation is fully applicable for nonlinear partial differential equations (Cotta et al., 2018), it might be a viable hybrid analytical–numerical approach to tackle more complicated reservoir problems such as multiphase flow (Clarkson et al., 2020) — including water, gas or water-alternating-gas (WAG) injection (Wang et al., 2021) — and pressure-dependent reservoir and fluid properties (Luo et al., 2018; Liu and Emami-Meybodi, 2021).

Nomenclature

Roman letters

$\mathbf{A}, \mathbf{B}, \mathbf{C}$: algebraic eigenvalue problem matrices in vector notation, dimensionless

A_{jk}, B_{jk}, C_{jk}: algebraic eigenvalue problem matrices in tensor notation, dimensionless

$\mathcal{B}$: GITT operator for the boundary condition

c_t: total compressibility, kPa^{-1}

d: generalized GITT formulation term, dimensionless

f: generalized GITT formulation initial condition, dimensionless

$f^+_{z,l}, f^-_{z,l}$: expressions defined in Eqs. (B.4) and (B.5), dimensionless

$F^+_{z,l}, F^-_{z,l}$: expressions defined in Eqs. (B.11) and (B.12), dimensionless

F_D: generalized GITT formulation filter expression, dimensionless

g: generalized GITT formulation source term, dimensionless

h_w: length of the perforated interval, m

H: Heaviside step function, dimensionless

$\mathbf{I}$: identity matrix, dimensionless

I_{jk}: integral of the auxiliary eigenvalues in Eq. (98), dimensionless

$I_X, I_Y, I_Z, I_{X'}, I_{Y'}, I_{Z'}$: one-dimensional components of Eq. (100) defined in Eqs. (101) and (102), dimensionless

$I_{\mathcal{X}}, I_{\mathcal{X}'}$: placeholders for the components in Eq. (100), defined in Eqs. (101) and (102), dimensionless

k: spherical equivalent permeability, mD

k_w: permeability in position $\mathbf{x_w}$, mD

k_x, k_y, k_z: permeability in directions x, y, z, mD

k_D: permeability multiplier in Eq. (4), dimensionless

$k_{D\mathrm{equiv}}$: long-term equivalent horizontal permeability in Eq. (137), dimensionless

$\mathbf{K}$: permeability tensor, mD

L: reference length, m

L_x, L_y, L_z: length of the domain in the x, y, z directions, m

$\mathcal{L}$: GITT operator for the differential equation

n: outward-facing normal unit vector to S

$N_{X_m}, N_{Y_m}, N_{Z_m}$: norms of the eigenfunctions in Eq. (69), dimensionless

N_{ψ_i}: norm of the eigenfunction ψ_i, dimensionless

N_{Ω_i}: norm of the auxiliary eigenfunction Ω_i, dimensionless

p: pressure, kPa

p_i: initial pressure, kPa

$\overline{\mathbf{p}}^*_{\mathbf{D}}$: vector of transformed potentials in Eq. (38), dimensionless

q: bottomhole volumetric flow rate, $\mathrm{m^3\,d^{-1}}$

r_w: well radius, m

r_D: expression defined in Eq. (B.3), dimensionless

R_D: distance to the point-source in Eq. (A.2), dimensionless

s: diffusivity equation source term geometry, $\mathrm{m^{-3}}$

S: the domain's external boundary

$\mathcal{S}$: length, area or volume of the source

t: time, h

T_{im}: expression defined in Eq. (110), dimensionless

υ_D: placeholder for x_D, y_D or z_D, dimensionless

V: problem formulation domain

w: weight function for the eigenfunctions' orthogonality property, dimensionless

$\mathbf{x}$: position vector (x, y, z), m

$\mathbf{x_w}$: position vector (x_w, y_w, z_w) of the well (source term), m

X, Y, Z: auxiliary one-dimensional eigenfunctions, dimensionless

$\mathcal{X}$: placeholder for auxiliary one-dimensional eigenfunctions, dimensionless

z^+_{wD}, z^-_{wD}: top and bottom coordinates of the limited entry perforation defined in Eq. (B.6), dimensionless

Greek letters

α: generalized GITT formulation boundary conditions coefficient, dimensionless

α_p: unit conversion factor, $1/2\pi$ in SI units and 141.2 in oilfield units

α_t: unit conversion factor, 1.0 in SI units and 0.000 263 74 in oilfield units

β: generalized GITT formulation boundary conditions coefficient, dimensionless

$\delta(x)$: Dirac delta, $\mathrm{m^{-1}}$

$\delta(\mathbf{x})$: three-dimensional Dirac delta, $\mathrm{m^{-3}}$

δ_{ij}: Kronecker delta, dimensionless

Δp: drawdown pressure $p - p_i$, kPa

$\Delta p'$: drawdown pressure logarithmic derivative, kPa

$\zeta_j(\mathbf{x_D})$: expression defined in Eq. (52), dimensionless

η: generalized GITT formulation auxiliary eigenvalues, dimensionless
η': change of variables used in simplifying Eq. (98), dimensionless
λ, γ, ν: auxiliary eigenvalues in directions x, y, z, dimensionless
μ: generalized GITT formulation eigenvalues, dimensionless
μ_f: viscosity, Pa s
ξ, ξ_e: placeholders in the Poisson summation formula in Eq. (71)
ξ_j: expression defined in Eq. (122), dimensionless
ρ: placeholder for auxiliary one-dimensional eigenvalues, dimensionless
τ: integration variable, dimensionless
ϕ: porosity, %
φ: generalized GITT formulation boundary condition, dimensionless
ψ: generalized GITT formulation eigenfunctions, dimensionless
Ω: generalized GITT formulation auxiliary eigenfunctions, dimensionless

Subscripts and superscripts

i, j, k, m, n, l: summation indices
i_x, i_y, i_z: one-dimensional indices corresponding to the three-dimensional index i
$\tilde{}$: normalization of the eigenfunction
$\hat{}$: refers to the auxiliary eigenvalue problem
$\bar{}$: transformed function
* : refers to the filtered problem
^{T} : transposed vector or matrix
$^{-1}$: inverse matrix
$_{ps}$: refers to the point-source
$_D$: dimensionless
$_w$: refers to the wellbore

CRediT authorship contribution statement

Leonardo O. Pelisoli: Conceptualization, Methodology, Software, Validation, Formal analysis, Writing – original draft, Writing – review & editing, Visualization. **Renato M. Cotta:** Methodology, Formal analysis, Resources, Writing – review & editing. **Carolina P. Naveira-Cotta:** Validation, Writing – review & editing, Supervision. **Paulo Couto:** Validation, Writing – review & editing.

Declaration of competing interest

The authors declare that they have no known competing financial interests or personal relationships that could have appeared to influence the work reported in this paper.

Acknowledgments

The authors are grateful to Petrobras and the Brazilian government agencies CNPq and FAPERJ for their support.

Appendix A. Point-source in a homogeneous reservoir by the method of images

The formulation in Eqs. (53)–(55) for the point-source in a closed homogeneous reservoir is usually solved in well testing literature through a two-step process: (i) calculate the point-source solution in an infinite domain; (ii) apply the *method of images* (Larsen, 1985) to create virtual boundaries in each direction by direct superposition of as many infinite domain solutions as required. The solution found in the literature for this process is (Ozkan and Raghavan, 1991)

$$p_D(\mathbf{x_D}, t_D) = \sum_{k=-\infty}^{+\infty}\sum_{m=-\infty}^{+\infty}\sum_{n=-\infty}^{+\infty}\sum_{p=1}^{2}\sum_{j=1}^{2}\sum_{l=1}^{2}\frac{1}{4\pi R_{Dpk,jm,ln}}\cdot \operatorname{erfc}\left(\frac{R_{Dpk,jm,ln}}{2\sqrt{t_D}}\right), \tag{A.1}$$

where

$$R^2_{Dpk,jm,ln} = (x_D + (-1)^p x_{wD} - 2kL_{xD})^2 + (y_D + (-1)^j y_{wD} - 2mL_{yD})^2 + (z_D + (-1)^l z_{wD} - 2nL_{zD})^2, \tag{A.2}$$

with time derivative

$$\frac{\partial p_D}{\partial t_D} = \frac{1}{(4\pi t_D)^{3/2}}\sum_{k=-\infty}^{+\infty}\sum_{m=-\infty}^{+\infty}\sum_{n=-\infty}^{+\infty}\sum_{p=1}^{2}\sum_{j=1}^{2}\sum_{l=1}^{2}\exp\left(-\frac{R^2_{Dpk,jm,ln}}{4t_D}\right). \tag{A.3}$$

By choosing an appropriate sorting order, Eqs. (A.1) and (A.3) can be rewritten as the single summation

$$p_D(\mathbf{x_D}, t_D) = \sum_{i=0}^{\infty}\frac{1}{4\pi R_{Di}(\mathbf{x_D})}\operatorname{erfc}\left(\frac{R_{Di}(\mathbf{x_D})}{2\sqrt{t_D}}\right), \tag{A.4}$$

$$\frac{\partial p_D}{\partial t_D} = \sum_{i=0}^{\infty}\frac{1}{(4\pi t_D)^{3/2}}\exp\left(-\frac{R^2_{Di}(\mathbf{x_D})}{4t_D}\right), \tag{A.5}$$

where each index i stands for a single combination of the original multiple summations. The most appropriate reordering criterion, in this case, is by increasing order of $R_{Di}(\mathbf{x_D})$, thus prioritizing those images closest to the point-source.

Appendix B. Limited entry vertical well in a homogeneous reservoir by the method of images

The solution for the limited entry vertical well in a homogeneous reservoir can be obtained by applying the superposition principle (Eq. (116)) directly to the point-source solution (Eq. (A.1)). This results in

$$p_D(\mathbf{x_D}, t_D) = \int_0^{t_D}\frac{\partial p_D}{\partial t_D}d\tau, \tag{B.1}$$

where the time derivative $\frac{\partial p_D}{\partial t_D}$ is given by

$$\frac{\partial p_D}{\partial t_D} = \sum_{k=-\infty}^{+\infty}\sum_{m=-\infty}^{+\infty}\sum_{n=-\infty}^{+\infty}\sum_{p=1}^{2}\sum_{j=1}^{2}\sum_{l=1}^{2}\frac{(-1)^l}{8\pi h_{wD} t_D}\cdot \exp\left(-\frac{r^2_{Dpk,jm}}{4t_D}\right)\left[\operatorname{erf}\left(\frac{f^+_{z,l}(z_D)}{2\sqrt{t_D}}\right) - \operatorname{erf}\left(\frac{f^-_{z,l}(z_D)}{2\sqrt{t_D}}\right)\right], \tag{B.2}$$

with

$$r^2_{Dpk,jm} = (x_D + (-1)^p x_{wD} - 2kL_{xD})^2 + (y_D + (-1)^j y_{wD} - 2mL_{yD})^2, \tag{B.3}$$

$$f^+_{z,l}(z_D) = z_D + (-1)^l z^+_{wD} - 2nL_{zD}, \tag{B.4}$$

$$f^-_{z,l}(z_D) = z_D + (-1)^l z^-_{wD} - 2nL_{zD}, \tag{B.5}$$

$$z^+_{wD} = z_{wD} + h_{wD}/2, \tag{B.6}$$

$$z^-_{wD} = z_{wD} - h_{wD}/2. \tag{B.7}$$

By choosing an appropriate sorting order, Eq. (B.2) can be rewritten as the single summation

$$\frac{\partial p_D}{\partial t_D} = \sum_{i=0}^{\infty}\frac{(-1)^{l(i)}}{8\pi h_{wD} t_D}\exp\left(-\frac{r^2_{Di}}{4t_D}\right)\cdot\left[\operatorname{erf}\left(\frac{f^+_{z,l(i)}(z_D)}{2\sqrt{t_D}}\right) - \operatorname{erf}\left(\frac{f^-_{z,l(i)}(z_D)}{2\sqrt{t_D}}\right)\right], \tag{B.8}$$

where each index i stands for a single combination of the original multiple summations. But unlike the classical point-source (Eq. (A.4)), creating a reordering criterion that adequately takes into account the z direction is difficult. Moreover, the τ integral in Eq. (B.1) does not have an analytical solution. Numerical integration was adopted for the

reference implementation of the present work, following the traditional procedure of independent summation of each orthogonal direction.

Finally, as already described in Section 4.3.1, an approximate infinite conductivity solution may be obtained by averaging Eqs. (B.1) and (B.8) along the wellbore, which results in

$$p_{wD}(x_D, y_D, t_D) = \int_0^{t_D} \frac{\partial p_{wD}}{\partial t_D} d\tau, \tag{B.9}$$

$$\frac{\partial p_{wD}}{\partial t_D} = \sum_{i=0}^{\infty} \frac{(-1)^{l(i)}}{8\pi h_{wD}^2 t_D} \exp\left(-\frac{r_{Di}^2}{4t_D}\right) \left\{ F^+_{z,l(i)}\left(z^+_{wD}, t_D\right) - \right.$$
$$\left. - F^+_{z,l(i)}\left(z^-_{wD}, t_D\right) - F^-_{z,l(i)}\left(z^+_{wD}, t_D\right) + F^-_{z,l(i)}\left(z^-_{wD}, t_D\right) \right\}. \tag{B.10}$$

which are no longer functions of z_D, and where

$$F^+_{z,l}(z_D, t_D) = 2\sqrt{\frac{t_D}{\pi}} \exp\left[-\left(\frac{f^+_{z,l}(z_D)}{2\sqrt{t_D}}\right)^2\right] + f^+_{z,l}(z_D)\,\mathrm{erf}\left(\frac{f^+_{z,l}(z_D)}{2\sqrt{t_D}}\right), \tag{B.11}$$

$$F^-_{z,l}(z_D, t_D) = 2\sqrt{\frac{t_D}{\pi}} \exp\left[-\left(\frac{f^-_{z,l}(z_D)}{2\sqrt{t_D}}\right)^2\right] + f^-_{z,l}(z_D)\,\mathrm{erf}\left(\frac{f^-_{z,l}(z_D)}{2\sqrt{t_D}}\right). \tag{B.12}$$

References

Almeida, A.R., Cotta, R.M., 1995. Integral transform methodology for convection–diffusion problems in petroleum reservoir engineering. Int. J. Heat Mass Transfer 38, 3359–3367. http://dx.doi.org/10.1016/0017-9310(95)00101-E, http://linkinghub.elsevier.com/retrieve/pii/001793109500101E.

Almeida, A.R., Cotta, R.M., 1996. Analytical solution of the tracer equation for the homogeneous five-spot problem. SPE J. 1, 31–38. http://dx.doi.org/10.2118/29218-PA.

Almeida, A.R., Cotta, R.M., 1999. On the integral transform solution of convection–diffusion problems within unbounded domain. J. Franklin Inst. 336, 821–832. http://dx.doi.org/10.1016/S0016-0032(99)00007-1.

Almeida, A.P., Naveira-Cotta, C.P., Cotta, R.M., 2020. Transient three-dimensional heat conduction in heterogeneous media: Integral transforms and single domain formulation. Int. Commun. Heat Mass Transf 117, 104792. http://dx.doi.org/10.1016/j.icheatmasstransfer.2020.104792, https://linkinghub.elsevier.com/retrieve/pii/S0735193320303201.

Barenblatt, G., Zheltov, I., Kochina, I., 1960. Basic concepts in the theory of seepage of homogeneous liquids in fissured rocks [strata]. J. Appl. Math. Mech. 24, 1286–1303. http://dx.doi.org/10.1016/0021-8928(60)90107-6.

Bidaux, P., Whittle, T.M., Coveney, P.J., Gringarten, A.C., 1992. Analysis of pressure and rate transient data from wells in multilayered reservoirs: Theory and application. In: Engineers, S.o.P. (Ed.), SPE Annu. Tech. Conf. Exhib. Society of Petroleum Engineers. http://dx.doi.org/10.2118/24679-MS.

Biryukov, D., Kuchuk, F.J., 2012a. Pressure transient solutions to mixed boundary value problems for partially open wellbore geometries in porous media. J. Pet. Sci. Eng. 96–97, 162–175. http://dx.doi.org/10.1016/j.petrol.2012.08.001.

Biryukov, D., Kuchuk, F.J., 2012b. Transient pressure behavior of reservoirs with discrete conductive faults and fractures. Transp. Porous Media 95, 239–268. http://dx.doi.org/10.1007/s11242-012-0041-x.

Carslaw, H.S., Jaeger, J.C., 1959. Conduction of Heat in Solids. Oxford University Press, Oxford.

Clarkson, C.R., Yuan, B., Zhang, Z., Tabasinejad, F., Behmanesh, H., Hamdi, H., Anderson, D., Thompson, J., Lougheed, D., 2020. Evaluation of the impact of multiphase flow on reservoir signatures in the wolfcamp shale. J. Nat. Gas Sci. Eng 76, 103187.

Cotta, R.M., 1986. Diffusion in media with prescribed moving boundaries: application to metals oxidation at high temperatures, in: II Lat. Am. Congr. Heat Mass Transf. Sã Paulo. pp. 502–513.

Cotta, R.M., 1990. Hybrid numerical/analytical approach to nonlinear diffusion problems. Numer. Heat Transf. Part B Fund. 17, 217–226. http://dx.doi.org/10.1080/10407799008961740.

Cotta, R.M., 1993. Integral Transforms in Computational Heat and Fluid Flow, first ed. CRC Press, Florida.

Cotta, R.M., 1994. Benchmark results in computational heat and fluid flow: The integral transform method. Int. J. Heat Mass Transfer 37, 381–393. http://dx.doi.org/10.1016/0017-9310(94)90038-8, https://linkinghub.elsevier.com/retrieve/pii/0017931094900388.

Cotta, R.M., Knupp, D.C., Naveira-Cotta, C.P., Sphaier, L.A., Quaresma, J.N.N., 2015. The unified integral transforms (unit) algorithm with total and partial transformation. Comput. Therm. Sci. An Int. J. 6, 507–524. http://dx.doi.org/10.1615/computthermalscien.2014008663.

Cotta, R.M., Knupp, D.C., Quaresma, J.N.N., 2018. Analytical methods in heat transfer. In: Kulacki, F.A. (Ed.), Handb. Therm. Sci. Eng.. Springer International Publishing, Cham, pp. 61–126. http://dx.doi.org/10.1007/978-3-319-26695-4_2.

Cotta, R.M., Mikhailov, M.D., 1997. Heat Conduction: Lumped Analysis, Integral Transforms, Symbolic Computation, first ed. Wiley, Hoboken, New Jersey.

Cotta, R.M., Mikhailov, M.D., 2005. Semi-Analytical Evaluation of Integrals for the Generalized Integral Transform Technique. In: 4th Work. Integr. Transform. Benchmark Probl. Rio de Janeiro, Brazil.

Cotta, R.M., Naveira-Cotta, C.P., Knupp, D.C., 2016. Enhanced convergence of eigenfunction expansions in convection–diffusion with multiscale space variable coefficients. Numer. Heat Transf. Part A Appl. 70, 492–512. http://dx.doi.org/10.1080/10407782.2016.1177342.

Couto, P., Marsili, M.D., 2013. A general analytical solution for the multidimensional hydraulic diffusivity equation by integral transform technique. In: OTC Bras. Offshore Technology Conference. pp. 1–20. http://dx.doi.org/10.4043/24319-MS.

Couto, P., Moreira, R., Marsili, M.D., 2011. A general analytical solution for the multidimensional transient linear hydraulic diffusivity equation in heterogeneous and anisotropic porous media. In: Conference, O.T. (Ed.), OTC Bras. Offshore Technology Conference. pp. 1–14. http://dx.doi.org/10.4043/22578-MS.

Deucher, R.H., Couto, P., Bodstein, G.C.R., 2016. Comprehensive solution for transient flow in heterogeneous porous media. Transp. Porous Media 113, 549–566. http://dx.doi.org/10.1007/s11242-016-0710-2.

Deucher, R.H., Couto, P., Bodstein, G.C.R., 2017. Transient solution for the energy balance in porous media considering viscous dissipation and expansion/compression effects using integral transforms. Transp. Porous Media 116, 753–775. http://dx.doi.org/10.1007/s11242-016-0799-3.

Dias, R.A.C., Chalhub, D.J.N.M., Oliveira, T.J.L., 2012. Analysis of Oil Displacement Through Water in Porous Media Using Integral Transforms and Cfd Package. In: 14th Brazilian Congr. Therm. Sci. Eng.

Ehlig-Economides, C., Ayoub, J.A., 1986. Vertical interference testing across a low-permeability zone. SPE Form. Eval 1, 497–510. http://dx.doi.org/10.2118/13251-PA.

Gerard, M.G., Horne, R.N., 1985. Effects of external boundaries on the recognition of reservoir pinchout boundaries by pressure transient analysis. Soc. Pet. Eng. J. 25, 427–436. http://dx.doi.org/10.2118/11141-PA.

Green, D.W., Willhite, G.P., 1998. Enhanced Oil Recovery, first ed. Henry L. Doherty Memorial Fund of AIME, SPE, Richardson, Texas.

Gringarten, A.C., Ramey, H.J., 1973. The use of source and green's functions in solving unsteady-flow problems in reservoirs. Soc. Pet. Eng. J. 13, 285–296. http://dx.doi.org/10.2118/3818-PA.

Herbert, R., 2016. The future of global energy: oil or gas?, in: APPEX Conf. London, UK. https://www.bp.com/en/global/corporate/news-and-insights/speeches/the-future-of-global-energy-oil-or-gas.html.

Hosseini, S.A., 2019. Fault leakage detection and characterization using pressure transient analysis. J. Pet. Sci. Eng. 176, 880–886. http://dx.doi.org/10.1016/j.petrol.2019.01.099.

Hovanessian, S., 1961. Pressure studies in bounded reservoirs. Soc. Pet. Eng. J. 1, 223–228. http://dx.doi.org/10.2118/50-PA.

IEA, 2021. World Energy Outlook 2021. Technical Report, IEA, Paris, https://www.iea.org/reports/world-energy-outlook-2021.

KAPPA, 2017. Rubis - numerical modeling, Érin 4.30.09b. https://www.kappaeng.com.

Kelvin, W.T., 1884. Mathematical and Physical Papers, Vol. 2. Cambridge University Press, Cambridge, UK.

Knupp, D.C., Cotta, R.M., Naveira-Cotta, C.P., Kakaç, S., 2015. Transient conjugated heat transfer in microchannels: Integral transforms with single domain formulation. Int. J. Therm. Sci 88, 248–257. http://dx.doi.org/10.1016/j.ijthermalsci.2014.04.017.

Kodhelaj, N., Shkëqim, B., 2016. Role of well testing and information in the petroleum industry- testing in multilayers reservoirs. Int. J. Eng. Sci. Comput 6, 1647.

Koshlyakov, N.S., 1936. Fundamental Differential Equations of Mathematical Physics, fourth ed. ONTI, Moscow.

Kuchuk, F.J., Habashy, T., 1997. Pressure behavior of laterally composite reservoirs. SPE Form. Eval 12, 47–56. http://dx.doi.org/10.2118/24678-PA.

Larsen, L., 1985. A simple approach to pressure distributions in geometric shapes. Soc. Pet. Eng. J 25, 113–120. http://dx.doi.org/10.2118/10088-PA.

Larsen, L., 1993. Pressure-transient behavior of reservoirs forming a pattern of coupled linear segments. In: Engineers, S.o.P. (Ed.), SPE Annu. Tech. Conf. Exhib. Society of Petroleum Engineers. http://dx.doi.org/10.2118/26459-MS.

Liu, Z., Emami-Meybodi, H., 2021. Rate transient analysis of infinite-acting linear flow by use of piecewise constant diffusivity coefficients. J. Pet. Sci. Eng 196, 107783. http://dx.doi.org/10.1016/j.petrol.2020.107783.

Luo, W., Tang, C., Feng, Y., Zhu, M., 2018. Mechanism of fluid flow along a dynamic conductivity fracture with pressure-dependent permeability under constant wellbore pressure. J. Pet. Sci. Eng 166, 465–475. http://dx.doi.org/10.1016/j.petrol.2018.03.059.

Mabrouk, M., 2014. Oil exploration costs on the rise. https://egyptoil-gas.com/features/oil-exploration-costs-on-the-rise.

Mavor, M., Walkup, G., 1986. Application of the parallel resistance concept to well test analysis of multilayered reservoirs. In: Engineers, S.o.P. (Ed.), SPE Calif. Reg. Meet. Society of Petroleum Engineers. http://dx.doi.org/10.2118/15117-MS.

Mikhailov, M.D., Ozisik, M.N., 1984. Unified Analysis and Solutions of Heat and Mass Diffusion, first ed. John Wiley & Sons, New York.

Naveira, C., Lachi, M., Cotta, R., Padet, J., 2009. Hybrid formulation and solution for transient conjugated conduction–external convection. Int. J. Heat Mass Transf 52, 112–123. http://dx.doi.org/10.1016/j.ijheatmasstransfer.2008.05.034, https://linkinghub.elsevier.com/retrieve/pii/S0017931008003694.

Naveira-Cotta, C.P., Cotta, R.M., Orlande, H.R.B., Fudym, O., 2009. Eigenfunction expansions for transient diffusion in heterogeneous media. Int. J. Heat Mass Transf 52, 5029–5039. http://dx.doi.org/10.1016/j.ijheatmasstransfer.2009.04.014, https://linkinghub.elsevier.com/retrieve/pii/S001793100900297X.

Nie, R.S., Zhou, H., Chen, Z., Guo, J.C., Xiong, Y., Chen, Y.Y., He, W.F., 2019. Investigation radii in multi-zone composite reservoirs. J. Pet. Sci. Eng 182, 106262. http://dx.doi.org/10.1016/j.petrol.2019.106262.

Nisle, R.G., 1958. The effect of partial penetration on pressure build-up in oil wells. Trans. AIME 213, 85–90. http://dx.doi.org/10.2118/971-G.

Ozisik, M.N., 1993. Heat Conduction, second ed. John Wiley & Sons, New York.

Ozkan, E., Raghavan, R., 1991. New solutions for well-test-analysis problems, orgname=Part 1-analytical considerations. SPE Form. Eval vol. 6, 359–368. http://dx.doi.org/10.2118/18615-PA.

Raghavan, R., 1995. The method of sources and sinks - a perspective. SPE Adv. Technol. Ser vol. 3, 135–143. http://dx.doi.org/10.2118/29617-MS.

Rahman, N.M.A., Bentsen, R.G., 2000. Use of an integral-transform technique for comprehensive solutions to transient-flow problems in homogeneous domains. In: Canada, P.S. (Ed.), Can. Int. Pet. Conf. Petroleum Society of Canada. http://dx.doi.org/10.2118/2000-042.

Rahman, N.M.A., Bentsen, R.G., 2001. In: Engineers, S.o.P. (Ed.), Comprehensive Solutions for Transient-Flow Problems in 3D Homogeneous Domains. SPE Middle East Oil Show, Society of Petroleum Engineers, http://dx.doi.org/10.2118/68139-MS.

Rahman, N.M.A., Bentsen, R.G., 2003. New analytical solutions for predicting pressure distribution and transient behavior in wedges and truncated wedges. SPE J. vol. 8, 280–290. http://dx.doi.org/10.2118/86195-PA.

Sagawa, A., Corbett, P.W., Davies, D.R., 2001. A semi-analytical pressure transient model for wells in heterogeneous linear reservoirs. In: Engineers, S.o.P. (Ed.), SPE Asia Pacific Oil Gas Conf. Exhib. Society of Petroleum Engineers. http://dx.doi.org/10.2118/68984-MS.

Satman, A., Eggenschwiler, M., Ramey, H.J., 1980. Interpretation of injection well pressure transient data in thermal oil recovery. In: Engineers, S.o.P. (Ed.), SPE Calif. Reg. Meet. Society of Petroleum Engineers. http://dx.doi.org/10.2118/8908-MS.

Shi, W., Cheng, S., Meng, L., Gao, M., Zhang, J., Shi, Z., Wang, F., Duan, L., 2020. Pressure transient behavior of layered commingled reservoir with vertical inhomogeneous closed boundary. J. Pet. Sci. Eng. vol. 189, 106995. http://dx.doi.org/10.1016/j.petrol.2020.106995, https://linkinghub.elsevier.com/retrieve/pii/S0920410520300917.

Silva-Lóez, D., Solano-Barajas, R., Turcio, M., Vargas, R., Manero, O., Balankin, A., Lira-Galeana, C., 2018. A generalization to transient bilinear flows. J. Pet. Sci. Eng vol. 167, 262–276. http://dx.doi.org/10.1016/j.petrol.2018.03.109, https://linkinghub.elsevier.com/retrieve/pii/S0920410518303036.

Sönichsen, N., 2021. Daily demand for crude oil worldwide from 2006 to 2020, with a forecast until 2026. https://www.statista.com/statistics/271823/daily-global-crude-oil-demand-since-2006.

Stewart, G., 2011. Well Test Design & Analysis. PennWell Corporation, https://books.google.com.br/booksid=9BWloRmrUYMC.

Streltsova-Adams, T., 1979. Pressure drawdown in a well with limited flow entry. J. Pet. Technol. 31, 1469–1476. http://dx.doi.org/10.2118/7486-PA.

Wachtmeister, H., Henke, P., Höök, M., 2018. Oil projections in retrospect. Appl. Energy vol. 220, 138–153. http://dx.doi.org/10.1016/j.apenergy.2018.03.013.

Wang, Y., Huerta, D.V., Kabir, C.S., Reza, Z., 2021. Immersive diagnostics of reservoirs under WAG injection, part I – understanding the dynamics around the injector. J. Pet. Sci. Eng. vol. 196, 107829. http://dx.doi.org/10.1016/j.petrol.2020.107829.

Warren, J., Root, P., 1963. The behavior of naturally fractured reservoirs. Soc. Pet. Eng. J vol. 3, 245–255. http://dx.doi.org/10.2118/426-PA.

Yaxley, L., 1987. Effect of a partially communicating fault on transient pressure behavior. SPE Form. Eval vol. 2, 590–598. http://dx.doi.org/10.2118/14311-PA.

Zhong, H., Yang, T., Yin, H., Lu, J., Zhang, K., Fu, C., 2020. Role of alkali type in chemical loss and ASP-flooding enhanced oil recovery in sandstone formations. SPE Reserv. Eval. Eng vol. 23, 431–445. http://dx.doi.org/10.2118/191545-PA.